11-2018

Seasonal and interannual assessment of cloud cover and atmospheric constituents across the Amazon (2000–2015): Insights for remote sensing and climate analysis

Vitor S. Martins
Iowa State University, vitors@iastate.edu

Evlyn M.L.M. Novo
National Institute for Space Research (INPE)

Alexei Lyapustin
NASA Goddard Space Flight Center

Luiz E.O.C. Aragão
University of Exeter

Saulo R. Freitas
NASA Goddard Space Flight Center

See next page for additional authors

Seasonal and interannual assessment of cloud cover and atmospheric constituents across the Amazon (2000–2015): Insights for remote sensing and climate analysis

Abstract

The quantitative assessment of cloud cover and atmospheric constituents improves our ability to exploit the climate feedback into the Amazon basin. In the 21st century, three droughts have already occurred in the Amazonia (e.g. 2005, 2010, 2015), inducing regional changes in the seasonal patterns of atmospheric constituents. In addition to climate, the atmospheric dynamic and attenuation properties are long-term challenges for satellite-based remote sensing of this ecosystem: high cloudiness, abundant water vapor content and biomass burning season. Therefore, while climatology analysis supports the understanding of atmospheric variability and trends, it also offers valuable insights for remote sensing applications. In this study, we evaluate the seasonal and interannual variability of cloud cover and atmospheric constituents (aerosol loading, water vapor and ozone content) over the Amazon basin, with focus on both climate analysis and remote sensing implications. We take the advantage of new atmosphere daily products at 1 km resolution derived from Multi-Angle Implementation for Atmospheric Correction (MAIAC) algorithm developed for Moderate Resolution Imaging Spectroradiometer (MODIS) data. An intercomparison of Aerosol Robotic Network (AERONET) and MAIAC aerosol optical depth (AOD) and columnar water vapor (CWV) showed quantitative information with a correlation coefficient higher than 0.81. Our results show distinct regional patterns of cloud cover across the Amazon basin: northwestern region presets a persistent cloud cover (>80%) throughout the year, while low cloud cover (0–20%) occurs in the southern Amazon during the dry season. The cloud-free period in the southern Amazon is followed by an increase in the atmospheric burden due to fire emissions. Our results reveal that AOD records are changing in terms of area and intensity. During the 2005 and 2010 droughts, the positive AOD anomalies ($\delta > 0.1$) occurred over 39.03% (240.3 million ha) and 27.14% (165.99 million ha) of total basin in the SON season, respectively. In contrast, the recent 2015 drought occurred towards the end of year (October through December) and these anomalies were observed over 23.72% (145 million ha) affecting areas in the central and eastern Amazon – unlike previous droughts. The water vapor presents high concentration values (4.0–5.0 g cm−2) in the wet season (DJF), while we observed a strong spatial gradient from northwestern to southeastern of the basin during the dry season. In addition, we also found a positive trend of water vapor content (~0.3 g/cm2) between 2000 and 2015. The total ozone typically varies between 220 and 270 DU, and it has a seasonal change of ~25–35 DU from wet season to dry season caused by large emissions of ozone precursors and long-range transport. Finally, while this study contributes to climatological analysis of atmospheric constituents, the remote sensing users can also understand the regional constraints caused by atmospheric attenuation, such as high aerosol loading and cloud obstacles for surface observations.

Keywords

Aerosol, Water vapor, Ozone, Cloud cover, MODIS-MAIAC, Climatology

Authors
Vitor S. Martins, Evlyn M.L.M. Novo, Alexei Lyapustin, Luiz E.O.C. Aragão, Saulo R. Freitas, and Claudio C.F. Barbosa

ISPRS Journal of Photogrammetry and Remote Sensing 145 (2018) 309–327

Contents lists available at ScienceDirect

ISPRS Journal of Photogrammetry and Remote Sensing

journal homepage: www.elsevier.com/locate/isprsjprs

Seasonal and interannual assessment of cloud cover and atmospheric constituents across the Amazon (2000–2015): Insights for remote sensing and climate analysis

Vitor S. Martins[a,b,*], Evlyn M.L.M. Novo[c], Alexei Lyapustin[d], Luiz E.O.C. Aragão[c,e], Saulo R. Freitas[f], Claudio C.F. Barbosa[a]

[a] Image Processing Division, National Institute for Space Research (INPE), São José dos Campos, SP, Brazil
[b] Agricultural and Biosystems Engineering, Iowa State University, Ames, IA, USA
[c] Remote Sensing Division, National Institute for Space Research (INPE), São José dos Campos, SP, Brazil
[d] NASA Goddard Space Flight Center, Greenbelt, MD, USA
[e] College of Life and Environmental Sciences, University of Exeter, EX4 4RJ, United Kingdom
[f] Universities Space Research Association/Goddard Earth Sciences Technology and Research at the Global Modeling and Assimilation Office, NASA Goddard Space Flight Center, Greenbelt, MD, USA

ARTICLE INFO

Keywords:
Aerosol
Water vapor
Ozone
Cloud cover
MODIS-MAIAC
Climatology

ABSTRACT

The quantitative assessment of cloud cover and atmospheric constituents improves our ability to exploit the climate feedback into the Amazon basin. In the 21st century, three droughts have already occurred in the Amazonia (e.g. 2005, 2010, 2015), inducing regional changes in the seasonal patterns of atmospheric constituents. In addition to climate, the atmospheric dynamic and attenuation properties are long-term challenges for satellite-based remote sensing of this ecosystem: high cloudiness, abundant water vapor content and biomass burning season. Therefore, while climatology analysis supports the understanding of atmospheric variability and trends, it also offers valuable insights for remote sensing applications. In this study, we evaluate the seasonal and interannual variability of cloud cover and atmospheric constituents (aerosol loading, water vapor and ozone content) over the Amazon basin, with focus on both climate analysis and remote sensing implications. We take the advantage of new atmosphere daily products at 1 km resolution derived from Multi-Angle Implementation for Atmospheric Correction (MAIAC) algorithm developed for Moderate Resolution Imaging Spectroradiometer (MODIS) data. An intercomparison of Aerosol Robotic Network (AERONET) and MAIAC aerosol optical depth (AOD) and columnar water vapor (CWV) showed quantitative information with a correlation coefficient higher than 0.81. Our results show distinct regional patterns of cloud cover across the Amazon basin: northwestern region presets a persistent cloud cover ($> 80\%$) throughout the year, while low cloud cover (0–20%) occurs in the southern Amazon during the dry season. The cloud-free period in the southern Amazon is followed by an increase in the atmospheric burden due to fire emissions. Our results reveal that AOD records are changing in terms of area and intensity. During the 2005 and 2010 droughts, the positive AOD anomalies ($\delta > 0.1$) occurred over 39.03% (240.3 million ha) and 27.14% (165.99 million ha) of total basin in the SON season, respectively. In contrast, the recent 2015 drought occurred towards the end of year (October through December) and these anomalies were observed over 23.72% (145 million ha) affecting areas in the central and eastern Amazon – unlike previous droughts. The water vapor presents high concentration values (4.0–5.0 g cm^{-2}) in the wet season (DJF), while we observed a strong spatial gradient from northwestern to southeastern of the basin during the dry season. In addition, we also found a positive trend of water vapor content (~ 0.3 g/cm^2) between 2000 and 2015. The total ozone typically varies between 220 and 270 DU, and it has a seasonal change of ~25–35 DU from wet season to dry season caused by large emissions of ozone precursors and long-range transport. Finally, while this study contributes to climatological analysis of atmospheric constituents, the remote sensing users can also understand the regional constraints caused by atmospheric attenuation, such as high aerosol loading and cloud obstacles for surface observations.

* Corresponding author.
E-mail addresses: vitor.martins@inpe.br (V.S. Martins), evlyn.novo@inpe.br (E.M.L.M. Novo).

https://doi.org/10.1016/j.isprsjprs.2018.05.013
Received 1 October 2017; Received in revised form 15 May 2018; Accepted 17 May 2018
Available online 24 May 2018

1. Introduction

The Amazon ecosystem plays a crucial role in the Earth's climate system. Several studies have shown the relevance of this ecosystem to climate feedback: fire and deforestation effects in the carbon budget (Aragão et al., 2014; Baccini et al., 2012), climate change and land-use transition (Malhi et al., 2008; Davidson et al., 2012; Nobre et al., 2016), vegetation function and traits (Hilker et al., 2015; Phillips et al., 2009), thermal and hydrological anomalies (Tomasella et al., 2010; Marengo and Espinoza, 2016; Jiménez-Muñoz et al., 2016). In this context, remote sensing data offer a viable means to explore spatial and temporal information, providing a range of insights about the tropical ecosystems (Chambers et al., 2007; Yang et al., 2013). The spectral indices and time series approaches have been widely used across the Amazon basin detecting seasonal changes of rainforest vegetation (Hilker et al., 2015; Moura et al., 2017), urban mapping (Lu et al., 2011), sediment dynamic in the rivers (Park and Latrubesse, 2014; Lobo et al., 2016), cropland and pasture monitoring (Arvor et al., 2012; Arantes et al., 2016; Aguiar et al., 2017). While optical sensors allow the synoptic view of the landscape dynamics (Barbosa et al., 2015), the top-of-atmosphere (TOA) radiance measured by satellite sensors is not only dependent on the ground properties, but is often distorted by atmospheric constituents (Okin and Gu, 2015; Vermote and Kotchenova, 2008).

The atmospheric attenuation imposes constraints on the radiometric quality of satellite-based observations, and an accurate atmospheric correction is often required to maintain the temporal consistence of this scientific data (Feng et al., 2013; Zhu, 2017). In the Amazon basin, the seasonal variability of main atmospheric constituents represents a challenge for optical remote sensing: (i) cloudiness regime, (ii) high aerosol burden in the dry season, (iii) seasonal water vapor and ozone concentration. Clouds are primary obstacle for surface observation in the tropical rainforest regions. Asner (2001) evaluated the probability of cloud-free images using the Landsat archive (1984–1997) and reported critical limitation for satellite observations over northern Amazon. Moreover, 3D adjacency effects distort the target reflectance when pixels are close to cloud borders or under undetectable thin cloud cirrus (Koren et al., 2007; Marshak et al., 2008). While cloudiness periods reduce the number of available cloud-free pixels, large amount of aerosol particles in the atmosphere causes severe distortions on the multispectral data. Zelazowski et al. (2011) simulated the atmospheric effects in the vegetation spectrum to emphasize the aerosol impact on the apparent reflectance. Likewise, Martins et al. (2017a) reported that atmospheric scattering might represent more than 84% of TOA reflectance over Amazon floodplain lakes. In contrast, the water vapor and ozone present absorption features in narrow wavelength intervals along the solar spectrum, such as 0.94, 1.14, 1.38 and 1.88 μm for water vapor; and 0.28, 0.31 and 0.58 μm for ozone (Gao et al., 2009).

Recent studies reported that uncertainties of atmospheric correction and cloud screening can lead to incorrect inferences about vegetation dynamic during drought years (Samanta et al., 2012; Hilker et al., 2012); although other factors may play a role, such as artefacts of sun-sensor geometry (Moura et al., 2012; Morton et al., 2014; Maeda and Galvão, 2015; Nagol et al., 2015). A controversial literature about Amazon greenness and drought sensitivity emerged in the past years. Saleska et al. (2007) observed an increase in the vegetation greenness during 2005 drought using Moderate Resolution Imaging Spectroradiometer (MODIS) C4 enhanced vegetation index (EVI) and concluded that intact Amazon forest is more drought-resistant and photosynthetic active than previously thought. Conversely, Samanta et al. (2010) claimed that poor data quality induced the apparent higher EVI anomalies observed in 2005, and Xu et al. (2011) observed vegetation browning in more than 50% of the forested area during 2010 drought, which contradicts the drought resilience hypothesis stated in the previous analysis of the 2005 drought. Some efforts, however, have been made to evaluate these uncertainties over tropical ecosystems. Recently, Hilker et al. (2012) reported notable noise effects on the current MODIS surface reflectance products due to aerosol contamination (dry season) and undetected clouds (wet season), which explain, at least in part, the discrepancies of greening and browning anomalies during drought years. While numerous studies have explored the built-in elements to reconcile the discussion about the sensitivity of Amazon rainforest to climate variability (Hilker et al., 2014; Maeda et al., 2014; Anderson et al., 2010; Brando et al., 2010; Morton et al., 2014), the atmospheric dynamic is also relevant to establish the linkage between seasonal variability and challenges for optical remote sensing data over the Amazon basin.

The Multi-Angle Implementation of Atmospheric Correction (MAIAC) is a novel algorithm developed for MODIS Collection 6 (C6) data (Lyapustin et al., 2011a). This algorithm applies a dynamical time series technique to derive the MODIS surface bidirectional reflectance factor and atmospheric retrievals at high 1 km resolution, such as aerosol optical depth (AOD), cloud masking and column water vapor (CWV) (Lyapustin et al., 2008; 2011b). Hilker et al. (2012) showed that MAIAC algorithm enhances the accuracy of cloud detection in this tropical ecosystem and increases the number of clear-sky observations compared with standard procedures. Additionally, Martins et al. (2017b) reported a high confidence of MAIAC AOD retrievals over vegetated surfaces and small negative bias at high AOD events (e.g. biomass burning). The authors also found that MAIAC CWV retrievals present expected error within 15% and correlation coefficient (R) of 0.968 with AERONET measurements.

The objective of this paper is to evaluate the seasonal and interannual variability of cloud cover and atmospheric constituents (aerosol, water vapor and ozone) with focus on both climate analysis and remote sensing implications. We used 15-year MODIS-MAIAC atmospheric products between 2000 and 2015 across the Amazon basin. The drought-induced changes in the atmospheric constituents are being presented. We also discuss the implications of seasonal atmospheric constituents into remote sensing applications; a question related to the better cloud-free period or atmospheric effects in the vegetation spectrum. As far as we know, this study is a novel assessment of atmospheric constituents using new MODIS-MAIAC products at high spatial resolution (1 km).

2. Background

The atmosphere dynamics in the Amazon basin is a synergetic system that has impacts on the regional and global climate (Emck, 2007; Nobre et al., 2009a). Rainforest's evapotranspiration and moisture inflow from the Atlantic Ocean are large-scale drivers of moisture recycling over the region (Spracklen et al., 2012; Boers et al., 2017). The easterly moisture-laden air is blocked in the eastern slope of central Andes Mountains (0–10° S) (Garreaud, 2009), and South America low-level jet transports high moisture content and aerosols towards the subtropical latitudes (Freitas et al., 2005; Vera et al., 2006). In the austral summer (DJF), South Atlantic Convergence Zone produces a regime of intense precipitation from southwestern Amazon toward western subtropical Atlantic Ocean (Carvalho et al., 2004; Vuille et al., 2012). Nonetheless, monsoon systems are extremely sensitive to mesoscale convective forces and land–ocean interaction. For instance, sea surface temperature (SST) variation in the Pacific Ocean controls the so-called El Niño Southern Oscillation (ENSO) events (Niño 3.4 at 5°N to 5°S latitude and 120° to 170°W longitude) (Grimm, 2011; Grimm and Tedeschi, 2009). In a most recent 2015–2016 drought, warming of eastern Pacific (El Niño) suppressed wet-season rainfall in the northern and eastern Amazonia and a record-breaking warming was observed over most part of Amazon basin (Jiménez-Muñoz et al., 2016).

Although extreme phases of ENSO modulate the climate variability and hydrological regimes in the Amazon basin, it is not the only mechanism controlling the interannual variability of the Amazon climate. The tropical Atlantic SST gradient has a strong regional influence on drought episodes: the warmer than average tropical North Atlantic

Fig. 1. Location of the Amazon basin. AERONET sites were used to validate MAIAC aerosol optical depth (AOD) and columnar water vapor (CWV) retrievals: Manaus-Embrapa (2.89°S, 59.96°W) and Rio Branco (9.95°S, 67.86° W).

shifts the Intertropical convergence zone (ITCZ) to northward position and reduces moisture flow over the Amazon basin (Yoon and Zeng, 2010; Grodsky and Carton, 2003; Sierra et al., 2015). For instance, the 2005 Amazon drought was mainly associated with warm tropical North Atlantic (latitude 10–15°N) and affected part of western Amazonia (Cox et al., 2008; Marengo et al., 2008). Therefore, these extreme droughts have been linked to (i) occurrence of El Niño episodes; (ii) strong warming of SST in tropical North Atlantic; or (iii) both together (Marengo and Espinoza, 2016, see references therein). On interannual timescales, these episodes produce large-scale shifts in the rainfall distribution leading to warming anomalies, fire disturbance and tree mortality Jiménez-Muñoz et al., 2013; Phillips et al., 2009).

In the Amazon context, fires are a common, fast and low-cost practice used for direct land clearing (Aragão et al., 2007; 2008), and their emissions can drastically change the aerosol concentrations during the burning season (Reddington et al., 2015). Although the fire emissions can be transported over several hundreds of kilometers (Hoelzemann et al., 2009), a strong correlation between high values of AOD and active fire counts was observed across the Amazon basin (Bevan et al., 2009; Koren et al., 2007). Similarly, Torres et al. (2010) reported the variability of AOD values with changes in the active fire counts (e.g. peak AOD in drought 2007 and decline during 2009 flood year). The recent droughts (e.g. 2005, 2010 and 2015) have raised the debate about fire emissions and forest carbon dynamics (Doughty et al., 2015; Nobre et al., 2016). Aragão et al. (2018) found that drought-induced forest fires prevail over those due to deforestation; fire emissions are losing their relation to the deforestation rates.

While fire emissions and air pollution affect the human health (Ignotti et al., 2010; Smith et al., 2014; Wiedinmyer, 2015), atmospheric composition also suffers substantial alterations driven by co-emission of trace gases including nitrogen oxides (NO_x), volatile organic compounds (VOCs), carbon dioxide (CO_2) and methane (CH_4) (Andreae and Merlet, 2001; Artaxo et al., 2013). These trace gases and other natural biogenic emissions are precursors of ozone (O_3) formation through photochemical reactions (Akagi et al., 2011; Jaffe and Wigder, 2012; Royal Society, 2008) and can alter the seasonal net tropospheric O_3 burden (Karl et al., 2007; Pacifico et al., 2015). Ziemke et al. (2009) showed an increased tropospheric O_3 during the fire season; it contributes with relative 6–7 DU to mean values (25–40 DU). Note that the tropospheric ozone represents a small fraction of total column ozone (~10%) and the seasonal variation is also driven by both dynamical and chemical processes in the stratosphere, with typical range between 220 and 235 DU in the tropics (Ziemke et al., 2011; Fioletov, 2008).

3. Data and methods

3.1. MODIS-MAIAC products: AOD, CWV and cloud mask

The Moderate Resolution Imaging Spectroradiometer (MODIS) instruments on board of Terra (~10:30 local time overpass) and Aqua (~13:30 overpass) platforms deliver historical and continuous Earth's observations since March-2000 and May-2002, respectively (Salomonson et al., 1989). These instruments are part of the NASA Earth Observation System (EOS) program developed to monitor the land and atmosphere systems. The MODIS sensor provides 36 spectral bands, spanning from 0.415 μm to 14.5 μm, large scan swath (~2330 km), nearly daily observation (temporal resolution of 1–2 days) and three spatial resolutions (250 m, 500 m or 1000 m). The

Table 1
Annual bias of MAIAC CWV used to correct the water vapor data in the time-series. These values are from Section 4.6 in Martins et al. (2017b).

CWV bias Terra (g cm^{-2})	2000	2001	2002	2003	2004	2005	2006	2007
	−0.289	−0.184	−0.198	−0.152	−0.218	−0.218	−0.095	−0.103
	2008	2009	2010	2011	2012	2013	2014	2015
	−0.012	0.053	0.062	0.129	0.123	0.175	0.163	0.301

MODIS data are processed in various levels (Level 0 to 4), and Level 1B products (geolocated and calibrated) are the inputs to geophysical algorithms. The results are known as Level 2 (L2) products, such as aerosol and water vapor. The success of the MODIS land–atmosphere products is associated with continuous efforts to provide high-quality data for scientific purposes. In this sense, newly available multi-angle MODIS algorithm, named MAIAC, implements a novel atmospheric correction approach based on dynamic time-series and block-pixel analysis, which improves the cloud screening and quality of aerosol retrievals. For time series analysis, MAIAC stores up to 16 days of MODIS C6 observations gridded at 1 km spatial resolution. Using these multi-angle observations of the same surface area over time, MAIAC algorithm is able to explore a certain level of stable surface background to make simultaneous retrievals of atmospheric aerosols and surface bidirectional reflectance factor from MODIS data. Currently, MAIAC C6 is operational and official MODIS-MAIAC products will be released soon. For detailed information about MAIAC's radiative transfer basis, atmospheric correction, cloud detection and aerosol algorithm, see Lyapustin et al. (2011a; 2011b; 2011c).

This study encompasses 12 MAIAC tiles over the Amazon basin (~6.1 million km^2), spanning 6°N to 20°S in latitude and 80°W to 49°W in longitude (Fig. 1). We use MAIAC Terra data due to the large number of satellites crossing the Equator at nearly the same local time, while data from Aqua are more affected by cloudiness from cumulus development (Hilker et al., 2015). Our current MAIAC dataset contains ~96.000 images between 2000 and 2015 for each atmospheric constituent: AOD at 550 nm (unitless), CWV (g cm^{-2}), and cloud masking at 1 km spatial resolution. The image processing involves the (i) extraction of scientific layers from HDF files, (ii) build a mosaic of all MAIAC tiles, and (iii) reprojection to World Geodetic System 84 (WGS84). The cloud mask is available into the Quality Assurance (QA) layer and this information was used to compute the fraction of cloud cover.

3.2. MODIS-MOD08 product: total column ozone

The MOD08 product is part of the MODIS/Terra Level-3 products and contains several atmospheric parameters, such as total column ozone burden, temperature, and atmospheric water vapor. All scientific data in this product are derived from statistical analysis of the MODIS Level-2 products (e.g. MOD07 for atmospheric profile), and these statistical results are stored into global grid of 1° × 1° resolution (Hubanks et al., 2015). Note, therefore, that MOD08 product is the subset information of MODIS L2 products, but it offers a unique opportunity for large-scale applications. In this study, we used the MOD08_D3 (daily) product from Collection 6 between 2000 and 2015. The total column ozone (TOZ) was extracted from scientific layer, called "Total_Ozone_Mean", rescaled to Dobson units (DU) by 0.1 factor, and then, the pixels were resized from 1° to 1 km resolution–only to overlay the MODIS-MAIAC dataset. The algorithm of total ozone content applies the primary information of MODIS channel 30 (9.6 μm) to solve the radiative transfer equation and performs the statistical regression with vertical atmospheric profiles (Borbas et al., 2011; Seemann et al., 2003). More information is available at Algorithm Theoretical Basis Documents (https://modis-images.gsfc.nasa.gov/_docs/MOD07_atbd_v7_April2011.pdf).

3.3. AERONET observations

AERONET (AErosol RObotic NETwork) is a global network of automatic sun-and-sky radiometers for aerosol monitoring (Holben et al., 1998). Direct sun measurements are used to compute the AOD values at seven wavelengths (340, 380, 440, 500, 675, 870, 1020 nm), while CWV retrievals are derived from the channel 940 nm (Schmid et al., 1996). The AOD is an optical measure of light extinction by aerosols in the atmospheric column (e.g. dust, smoke, pollution) and can be useful for air quality analysis. The AERONET data are available with cloud-screened and quality-assured at Level-2 products. In this study, we compare MAIAC and AERONET L2 records for AOD and CWV acquired at Manaus-Embrapa (2.89°S, 59.96°W) and Rio Branco (9.95°S, 67.86°W) sites (Fig. 1). Despite the large variety of aerosol types and loading across the Amazon, these AERONET sites are appropriate options to represent distinct aerosol context using long-term records. Here, AERONET AOD values were interpolated to a 550 nm using quadratic fits on a log–log scale (Eck et al., 1999), and thus, the averaged AERONET AOD taken within ± 30 min of satellite overpass was compared to averaged MAIAC values within 25 × 25 km^2 box centered at the site. The statistical analysis of MAIAC and AERONET comparison includes the coefficient of correlation (R), slope of linear regression (S_o) and root mean square error (RMSE).

While this comparison supports the reliability of these new atmospheric products, a comprehensive validation of MAIAC AOD and CWV was performed across South America (Martins et al., 2017b). The authors reported a systematic upward trend in CWV Terra retrievals as evidence of calibration drift along the MODIS/Terra mission. To address this trend issue, we used the mean bias per year (Table 1) to remove the potential error in the MAIAC CWV data.

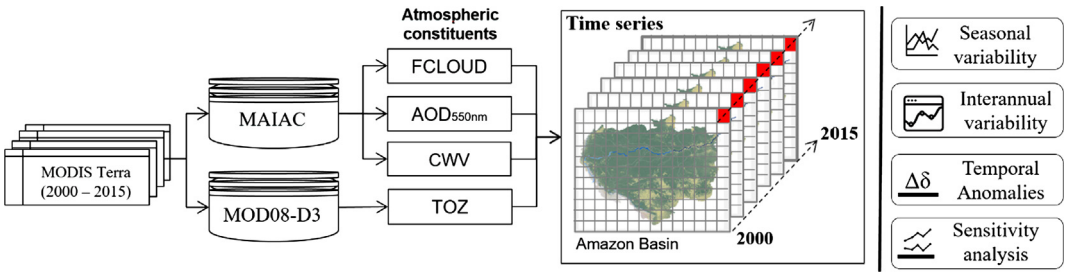

Fig. 2. Block diagram of spatiotemporal analysis of 15-year MODIS-MAIAC data: fraction of cloud cover (FCLOUD, %); aerosol optical depth at 550 nm ($AOD_{550\ nm}$, unitless); columnar water vapor (CWV, g cm^{-2}); total columnar ozone (TOZ, Dobson Units).

3.4. Data analysis

The historical and full dataset over Amazon basin allows image processing using several time-scales and spatial coverage (Fig. 2). We derived an averaged time-series data for all pixels (1 × 1 km) covering the Amazon basin. The frequency of cloud cover per pixel gives the fraction of cloud cover at distinct timescales (seasons and monthly). In addition to the averaged data, we computed the non-standardized anomalies (Δδ) using Eq. (1):

$$\Delta\delta_t = \mu_{t,year} - \langle \mu_t \rangle_{2000-2015} \quad (1)$$

where μ is the atmospheric constituent, $\mu_{t,year}$ is the average of the atmospheric constituent for t time for each year (2000, 2001,…, 2014, 2015); t time are seasons (DJF, MAM, JJA, SON) or monthly (Jan, Feb, …, Nov, Dec) averages, $\langle \mu_t \rangle_{2000-2015}$ is the averaged value over t time derived from all data (2000–2015).

The overall analysis was developed for two spatial scales: Amazon basin and regional analysis, hereafter AMZ (Section 4.3). The location of AMZ regions is based on the annual cumulative rainfall from 15-year Tropical Rainfall Measuring Mission (TRMM) 3B43-v7 product at 0.25° spatial resolution (Huffman et al., 2007).

Space-borne optical remote sensing is complex in nature and bounded by intrinsic uncertainties on it measurements, such as sensor degradation, radiometric calibration, directional effects of sun-view geometries and atmospheric attenuation (Okin and Gu, 2015). To provide insights about atmospheric effects, we performed a sensitivity analysis using the Second Simulation of a Satellite Signal in the Solar Spectrum–vector (6SV) model (Vermote et al., 1997). The 6SV is a robust and well-known radiative transfer model, and we simulate the atmospheric attenuation, affecting standard green vegetation spectrum, under two atmospheric conditions: (i) dry season (September 2005) and (ii) wet season (November 2014).

4. Results

4.1. Comparison of MAIAC and AERONET observations

Figs. 3 and 4 present the comparison between MAIAC and AERONET for AOD and CWV retrievals, respectively, over (a) Manaus-Embrapa and (b) Rio Branco sites (See location in Fig. 1). These two AERONET sites represent distinct aerosol and water vapor contexts. For example, Manaus-Embrapa site is close to dense forests and populated capital of Amazonas/Brazil, while Rio Branco site records the seasonal biomass burning events near deforested and agricultural areas. The results in Figs. 3 and 4 are based on match-ups between 2011 and 2015.

The AERONET AOD records vary between the climate seasons in the Rio Branco with 0.6–1.2 values from July to September due to anthropogenic fires in the region. In contrast, AOD records are typically lower than 0.4 over Manaus-Embrapa, even with urban emissions and local emissions near Manaus city. In general, our results show that MAIAC AOD retrievals agree well with ground-measurements in both AERONET sites. The time-series agreement illustrates the feasibility of MAIAC retrievals to trend the seasonal variability of AOD values in either clean or turbid condition, with a correlation coefficient (R) of 0.88 (Manaus) and 0.97 (Rio Branco) (Fig. 3). The peak September in the Rio Branco was observed in MAIAC retrievals and the impact of error (RMSE: ~0.065) becomes less relevant for high values when compared to low AOD events.

The comparison of MAIAC and AERONET CWV observations are shown in Fig. 4. In general, AERONET CWV records range from 3.0 to 4.5 g/cm^2 in Manaus site, while the seasonal variation is better observed in the Rio Branco site (2.5 to 4.5 g/cm^2). In overall, the seasonal variability of water vapor was fairly characterized by MAIAC retrievals, showing similar trend of AERONET records. Our findings also show that CWV retrievals have a better agreement with AERONET Rio Branco (R: 0.92) than those of Manaus site (R: 0.81). However, these retrievals are slightly higher when compared to AERONET records, with RMSE value

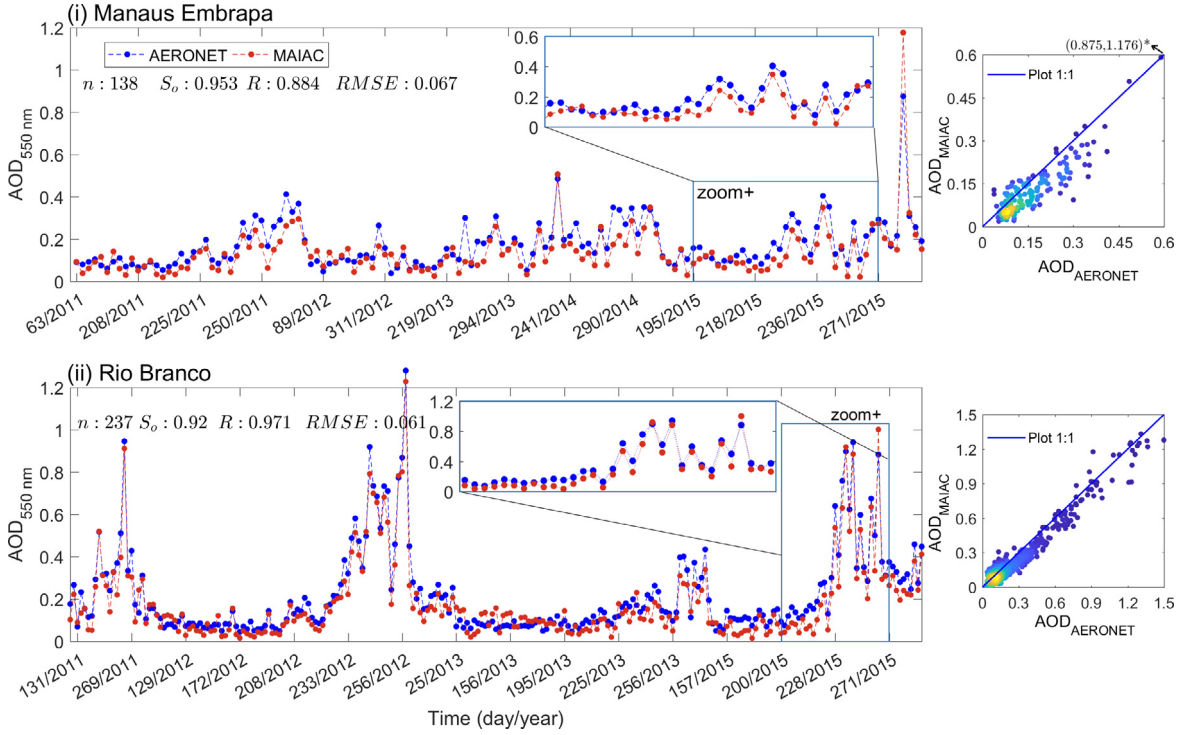

Fig. 3. Temporal analysis of MAIAC and AERONET AOD records from (a) Manaus and (b) Rio Branco between 2011 and 2015. Note that x-axis is irregular and some periods might present only a few points. The n value corresponds the number of match-ups between satellite product (MAIAC) and ground-truth (AERONET), S0 is the slope of linear regression, correlation coefficient (R) and root-mean-square-error (RMSE) between MAIAC and AERONET records.

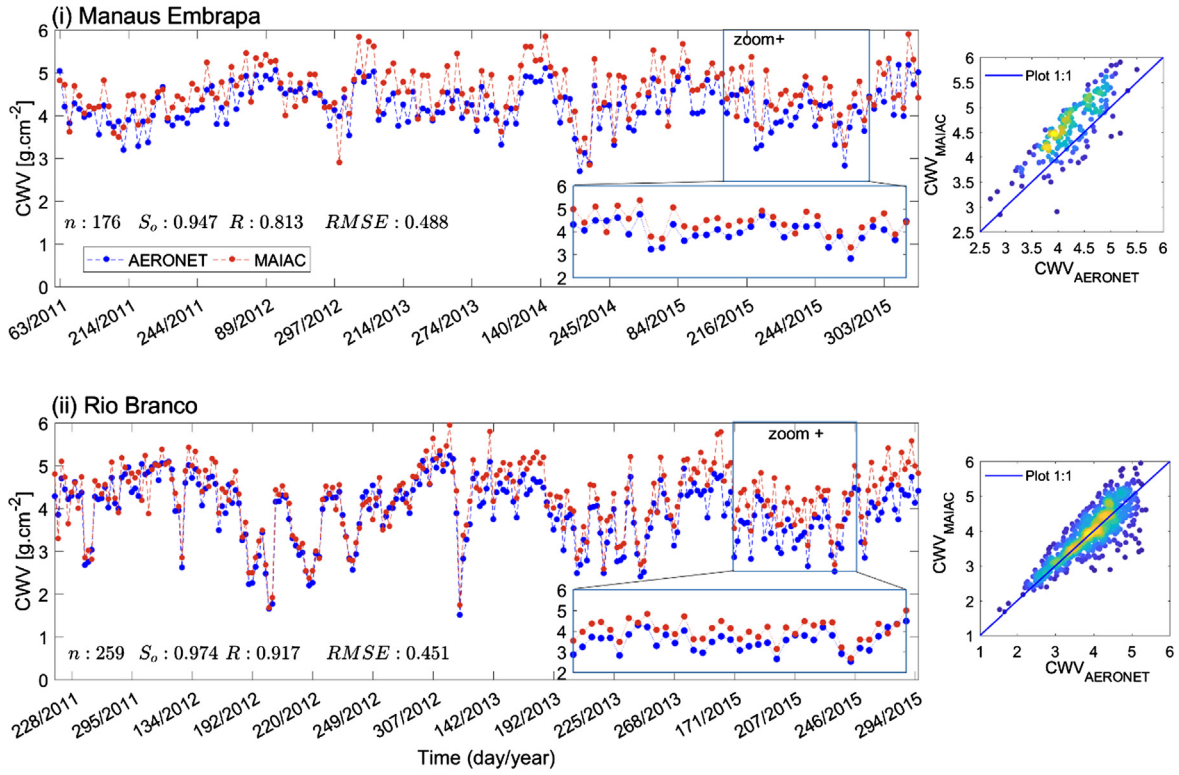

Fig. 4. The same as Fig. 3, but for columnar water vapor (CWV).

of 0.488 (Manaus) and 0.455 g/cm^2 (Rio Branco). Some peak retrievals were observed for high water vapor in the MAIAC retrievals, while AERONET records (Manaus) showed a lower variation in the same period.

4.2. Spatiotemporal patterns of atmospheric constituents

In this session, we present the spatial and temporal variability of each constituent across the Amazon using the averaged data over 2000–2015. In general, all constituents present spatial variation and seasonal changes across the Amazon: high cloud cover and water vapor values were observed during austral summer (DJF), while aerosol loading and total ozone content increase in the austral spring (SON) (Fig. 5). The north–south spatial gradient is also observed in the basin as result of regional climatology, landscape features and anthropogenic fires. In the summer season (DJF), high cloud cover (> 90%) reaches around 60.4% of the Amazon basin, while it decreases to ~5% during spring season (SON). We also observed that cloud cover is higher than 60% near the latitude range 2.5° S–5°N due to position of ITCZ cloudiness near the equator. On the northern sub-basins (e.g. Napo-Putumayo-Javari and Negro basins), the cloudiness persists mostly during 9 months (October to June) and imposes limitations for clear-sky observations. In contrast, southern sub-basins (e.g. High-Madeira and Tapajos basins) present up to 40% of cloud cover fraction between June and September (Fig. 5a), which is a potential window for remote sensing applications. Therefore, while near-constant cloudiness occurs in the northern Amazon, our results show seasonal variation of cloud cover over southeastern Amazon, spanning 5°S to 20°S in latitude and 65°W to 50°W in longitude. However, when the cloud coverage decays in the southern Amazon during JJA season, we also observed the peak AOD records at 1–2 months later (Fig. 5b).

Regional fire emissions increase the atmosphere burden during the spring season (SON) (Fig. 5b). The high AOD records (> 0.2) cover 57.1% of total basin, with most affected areas in the southern Amazon. Here, note that long-range transport of fire smokes changes the background aerosol over hundreds of kilometers from their sources, and spatial distribution of AOD records might lead to misinterpretation of local fire sources. While the burning season has a significant influence on the seasonal trend of aerosol burden, the northern Amazon (3°S to 10°N latitude) presents relative low and stable AOD condition (up to 0.2) throughout the year. Fig. 5c shows that water vapor typically ranges between 2.0 and 5.0 g/cm^2, with the maximum CWV over the northern Amazon (5° S–5°N in latitude). In general, water vapor content decreases substantially from northwestern to southeastern Amazon, although Andes Mountain (e.g. westernmost) shows the lowest concentrations (< 2.0 g/cm^2). During austral winter (JJA), the water vapor reduces to lower than 3.5 g/cm^2 over southern Amazon. For instance, High-Madeira basin presents lower CWV concentrations (2.5 to 3.5 g/cm^2) compared to all sub-basins in this season. In contrast, the northwestern and central Amazon present low seasonal variation of water vapor content, with values higher than 4.0 g/cm^2 throughout the year.

Fig. 5d shows that the total ozone presents relative low records (240–255 DU) in autumn (MAM), and increases to ~255–265 DU in the austral autumn (MAM) over the most part of Amazon. In the dry season, net radiation and trace gases contribute to increase the tropospheric ozone content (Ziemke et al., 2009), but this variation (↑ ~20 DU) is also a function of other factors as previously discussed. Note that aerosol burden and ozone content increase at the period over the southern sub-basins, while the northwestern basin shows a lower variability raging between 245 and 255 DU over all seasons (Fig. 5d). Tropical forest is a notable source of atmospheric BVOCs (Jardine and Jardine, 2016), and these results over pristine forest region suggested that natural VOCs and NOx emissions (+ net radiation) might control the tropospheric O_3 production in the region (Karl et al., 2007).

4.3. Regional analysis

To investigate these atmospheric constituents at the regional scale, we performed the seasonal and interannual assessment over four Amazon regions, called AMZs (Fig. 6a). These regions are located over

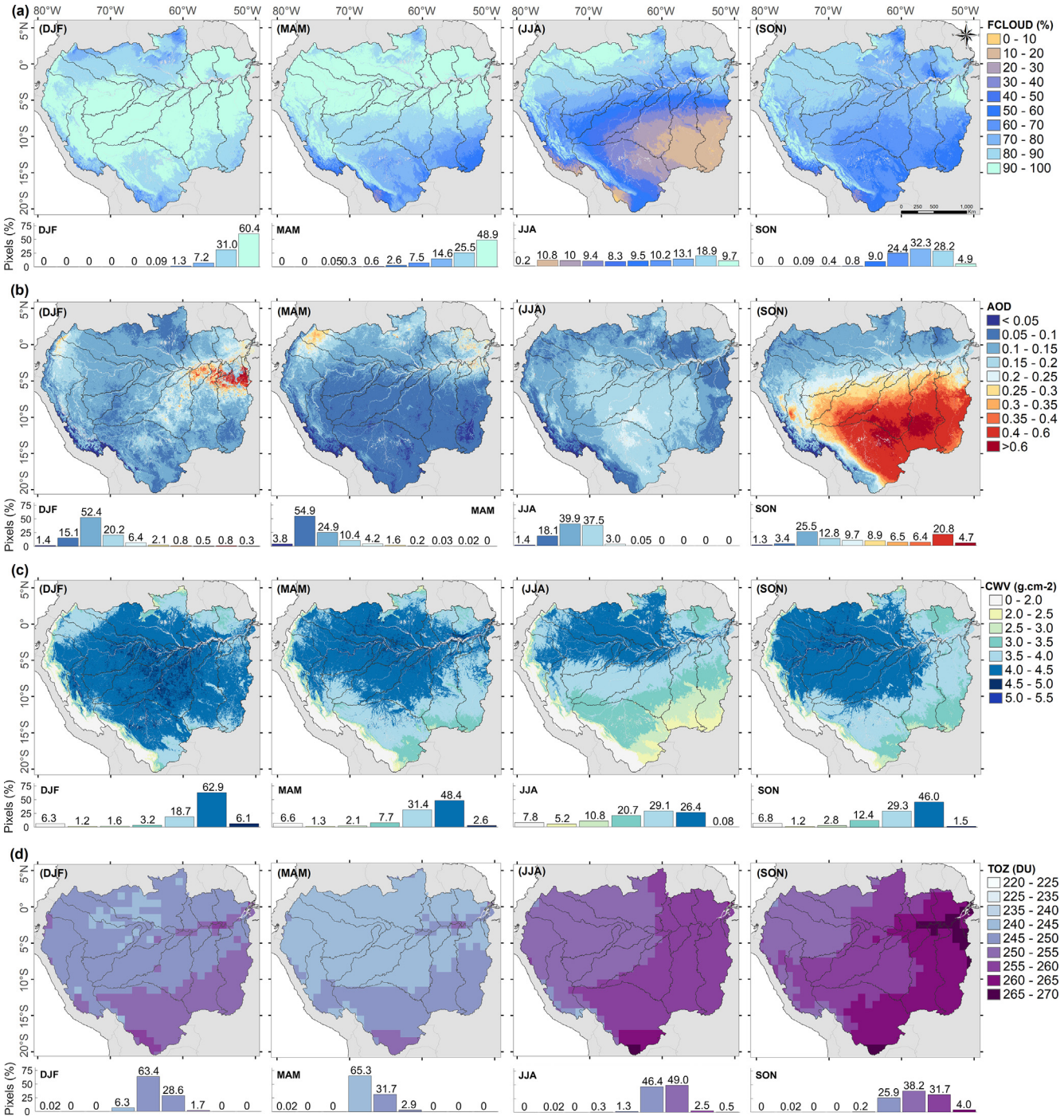

Fig. 5. Seasonal distribution of atmospheric constituent in the Amazon basin. The panels present each atmospheric constituent: (a) cloud cover fraction (FCLOUD, %); (b) aerosol optical depth at 550 nm (AOD_{550}, unitless); (c) columnar water vapor (CWV, g/cm^2); (d) total columnar ozone (TOZ, Dobson Units). The colored bars represent the pixel counts (%) for each concentration – similar sequence of legend.

areas sensitive to rainfall variations. The normalized coefficient of variation (CV_{norm}) is the annual standard deviation of precipitation divided by its average. This coefficient was normalized between 0 and 1, and represents the annual variability of rainfall, ranging from low (0.0) to high variability (1.0). In general, the annual precipitation is typically around 1600–3000 mm for the most part of the Amazon. The highest annual rainfall occurs over the Northwestern (AMZ1) with ~3375 mm/year, and it changes gradually towards the Southeastern Amazon (AMZ4) reaching ~1740 mm/year. In the AMZ1 region, the annual precipitation is evenly distributed throughout the year (CV_{norm} of 0.1–0.2) and the rainy season occurs from March to June (Fig. 6b). While AMZ1 region presents regular rainfall during the year, high variability occurs over the other regions: central Amazon presents an annual CV_{norm} of 0.4–0.6, which increases to CV_{norm} higher than 0.6 towards the southwestern and southern Amazon. In addition, precipitation regime of AMZ2 region shows the concentration of annual rainfall of ~35.2% in the austral summer (DJF) compared to 11.4% during winter season (JJA). In addition, southern Amazon (AMZ4) has a well-defined rainy season during summertime, with cumulative rainfall of ~790 mm (or 45.4% of total). In the AMZ3 region, austral autumn (MAM) presents 40% of annual rainfall (wet season) compared to 9.4% between June and September.

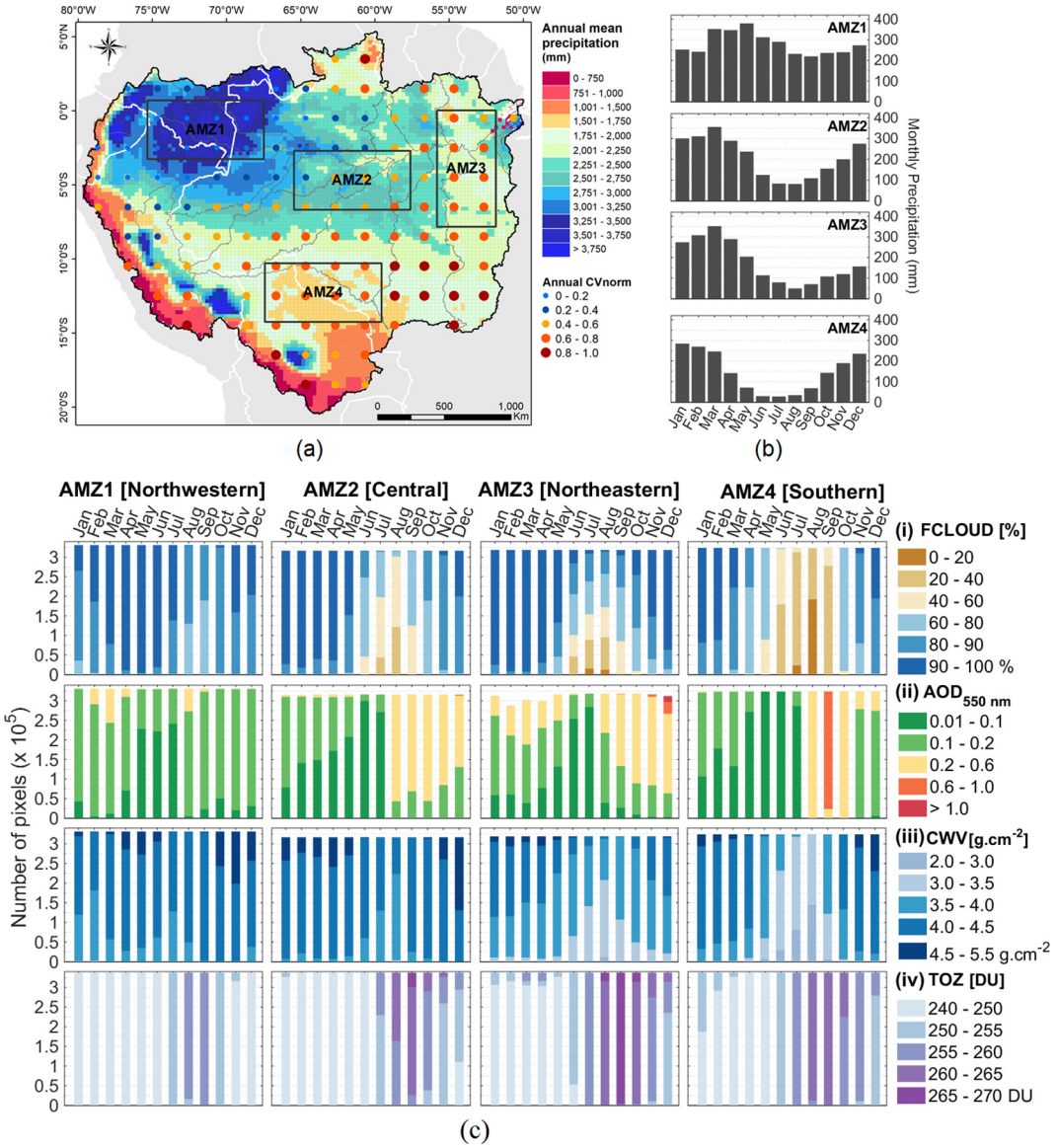

Fig. 6. Monthly average of precipitation and atmospheric constituents using a 15-year time series in the four regions. (a) Annual precipitation and normalized coefficient of variation (CV_{norm}) were calculated based on monthly mean from Tropical Rainfall Measuring Mission (TRMM). (b) Monthly precipitation was calculated from average TRMM data (2000–2015); (c) Monthly cloud cover fraction and atmospheric constituents from averaged MAIAC data (2000–2015). The y-axis of panels (c) shows the number of pixel for each concentration range: (i) fraction of cloud cover, (ii) aerosol optical depth at 550 nm, (iii) total precipitable water, (iv) total columnar ozone. The bounding box of four regions are described using upper left (UL) and bottom right (BR): AMZ1 (UL: 0.69°N/75.33°W and BR: 3.37°S/67.49°W); AMZ2 (UL: 2.69°S/65.46°W and BR: 6.64°S/57.61°W); AMZ3 (UL: 0.02°S/55.81°W and BR: 7.79°S/51.86°W) and AMZ4 (UL: 10.27°S/67.39°W and BR: 14.23°S/59.58°W).

Since the precipitation regime is a proxy for cloudiness in Amazon, it seems plausible that cloud cover is seasonally dependent in the region. For instance, our findings show that the rainy season in the AMZ2 region (6-month) is coincident with high cloud cover period (See Fig. 6b and ci). In the northwestern region, cloud cover is intense (~60–100%) as well as the precipitation rates, which restrict continuous surface observation by satellite images. In turn, cloud cover fraction changes rapidly in the other three regions during austral spring (SON). The southern region (AMZ4) presents the relative low cloud cover between June and September (~17 to 38%), although it increases to ~91% with the onset of the wet season (DJF). In addition, northeastern region (AMZ3) shows the highest cloud cover during March through May, when ITCZ is in its southernmost position (Fu et al., 2001; Grodsky and Carton, 2003).

Fig. 7 presents the seasonal non-standardized anomalies ($\Delta\delta_s$) between JJA/2000 and SON/2015 with drought and flood years (shaded). Note that Table 2 shows the seasonal averaged data for each constituent and readers are able to calculate the absolute values in the time series. The critical negative anomalies of cloud cover are clearly observed during drought years, where the $\Delta\delta$ ranges between −5 and −15% (Fig. 7a). In turn, flood years have experienced positive anomalies up to +8.5%, except in 2012. These extreme anomalies are rather expected during drought and flood years, while the regular variability of cloud cover ranges between −5 and 5%. Fig. 6ci suggests that most of the cloud-free period occurs between June and September. However, despite the increase in the probability of cloud-free images, the same period presents the highest concentrations of AOD (Fig. 6cii) and TOZ (Fig. 6civ), thus demonstrating how challenging is the interpretation of satellite information during the dry season, and particularly in drought conditions. Fig. 6cii shows that aerosol burden increases from 0.01 to 0.2 values to 0.2–0.6 between DJF and SON, except for AMZ1. In Southern Amazon (AMZ4) open fire is often used for land management

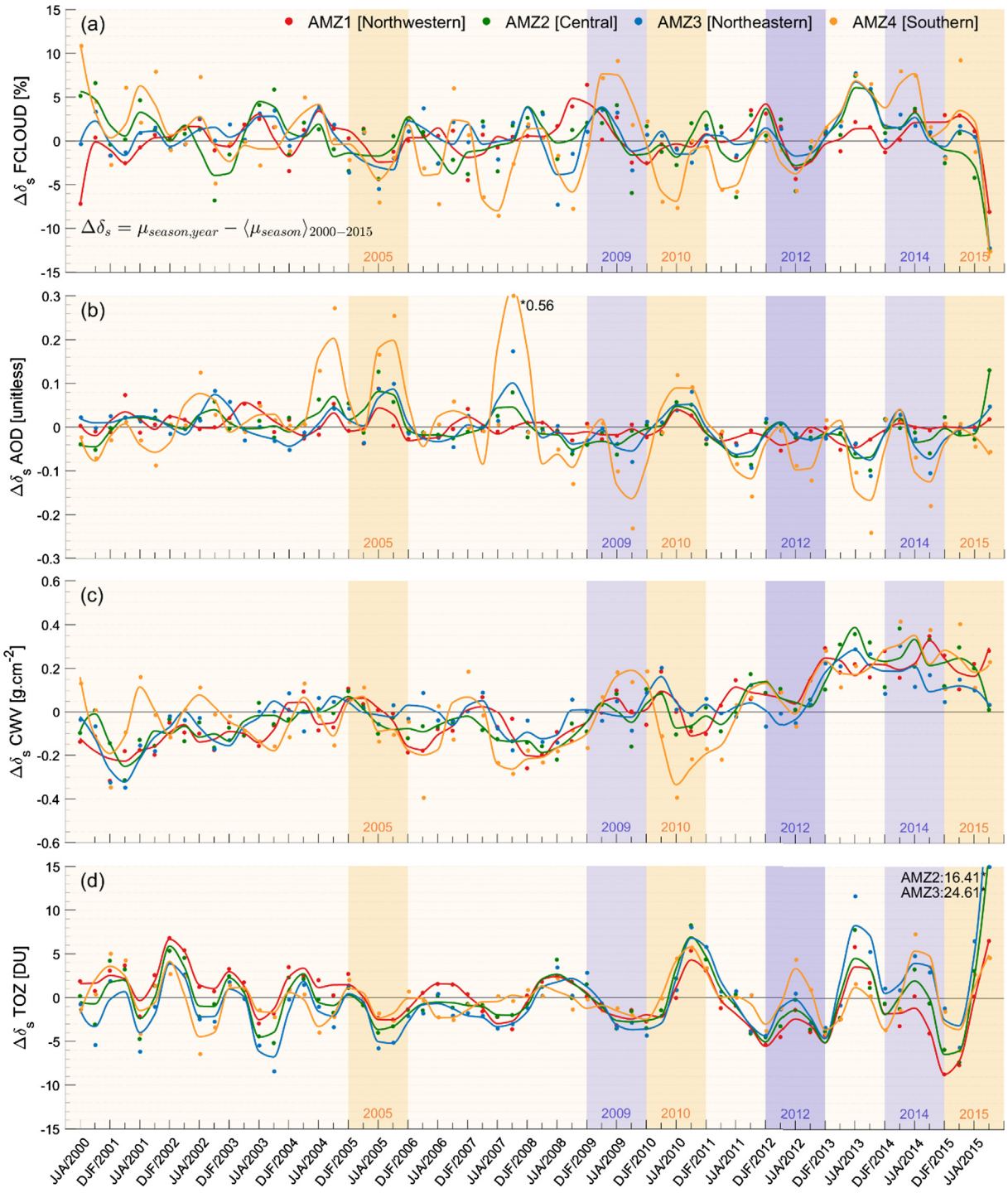

Fig. 7. Time-series of seasonal non-standardized anomalies ($\Delta\delta_s$) for atmospheric constituents in the four regions. (a) Fraction of cloud cover (FCLOUD, %). (b) Aerosol optical depth at 550 nm (AOD, unitless). (c) Columnar water vapor (CWV, g/cm^2). (d) Total columnar ozone (TOZ, Dobson units). The shaded bars are reference for drought years (brown) and flood years (blue) (Marengo and Espinoza, 2016). (For interpretation of the references to colour in this figure legend, the reader is referred to the web version of this article.)

of pastures and deforested areas during the dry season (Aragão et al., 2014) which can explain the AOD peaks reaching records higher than 0.6 in September (Fig. 6cii). In turn, fire practices are commonly observed at the end of the dry season over northeastern (AMZ3), causing relative high AOD events during November and December. In addition, our results in Fig. 7b shows that drought years are tipping points for aerosol burden, especially, 2005 and 2007; but it is changing in recent years. Note that it is possible to observe a decrease in AOD anomalies since 2010, which is a positive measure for air quality and forest fires in the Amazon basin.

Our findings in Fig. 6c show a similar seasonal pattern of aerosol loading and ozone content over most of the regions; high records are often observed in the second half of year. The increase of ozone content occurs from July to September, while the lowest records are from February to May. This pattern might be associated with long-range transport and environmental factors, such as net radiation and trace gases (CO, NOx and VOCs), which control the variability between wet and dry season (Royal Society, 2008). Further, ozone gradient presents

Table 2
Seasonal variability of cloud cover and key atmospheric constituent over the four regions. The values (average ± standard deviation) were calculated from 15-year MODIS-MAIAC products and standard MOD08 product.

	AMZ1	AMZ2	AMZ3	AMZ4		AMZ1	AMZ2	AMZ3	AMZ4
	FCLOUD (%)					CWV ($g\,cm^{-2}$)			
DJF	88.36 ± 3.2	92.33 ± 1.9	95.04 ± 3.5	91.35 ± 2.6	DJF	4.20 ± 0.19	4.40 ± 0.13	4.08 ± 0.22	4.29 ± 0.2
MAM	92.86 ± 1.1	91.23 ± 2.1	93.04 ± 3.8	75.72 ± 4.9	MAM	4.31 ± 0.16	4.45 ± 0.13	4.15 ± 0.25	4.07 ± 0.21
JJA	88.14 ± 3.0	57.22 ± 10.3	60.74 ± 21.5	29.25 ± 6.6	JJA	4.15 ± 0.13	4.05 ± 0.15	3.62 ± 0.27	3.20 ± 0.24
SON	85.11 ± 2.0	75.56 ± 3.4	80.30 ± 9.4	62.06 ± 3.1	SON	4.40 ± 0.1	4.30 ± 0.10	3.73 ± 0.2	3.99 ± 0.19
	AOD (unitless)					TOZ (DU)			
DJF	0.13 ± 0.02	0.14 ± 0.03	0.17 ± 0.05	0.12 ± 0.03	DJF	245.44 ± 0.6	247.1 ± 1.3	248.8 ± 1.8	250.85 ± 1.2
MAM	0.14 ± 0.04	0.1 ± 0.02	0.14 ± 0.06	0.08 ± 0.02	MAM	242.68 ± 0.3	244.1 ± 1.1	246.2 ± 2.4	246.56 ± 0.9
JJA	0.12 ± 0.02	0.14 ± 0.02	0.10 ± 0.03	0.17 ± 0.02	JJA	251.61 ± 0.3	254.3 ± 0.9	257.3 ± 0.5	256.48 ± 0.7
SON	0.13 ± 0.02	0.25 ± 0.04	0.27 ± 0.11	0.42 ± 0.05	SON	252.06 ± 0.8	258.0 ± 2.1	262.7 ± 1.9	259.45 ± 0.9

distinct amplitudes among these regions: southern (AMZ4) and northeastern (AMZ3) showed higher ozone content and variability than those in other two regions (AMZ1 and AMZ2). In the early wet season, the ozone content decreases from ~265 DU to ~245 DU, and the maximum gradient is of ↓35 DU from austral spring (SON) to autumn (MAM) season in the northeastern Amazon. Our results in Fig. 7d present that annual peak of $\Delta\delta_s$ occurs typically in JJA season and highest records were observed in 2015 drought followed by a significant decline in the cloud cover.

The cross-equatorial flow from the Atlantic Ocean and evapotranspiration of tropical contribute to a large amount of water recycling in the atmosphere (Wang and Fu, 2002; Marengo, 2006). Fig. 6ciii shows that northwestern (AMZ1) and central (AMZ2) regions have a near-constant CWV concentration of ~3.5–4 g/cm^2, and in contrast, northeastern (AMZ3) and southern (AMZ4) present a drastic decrease of CWV with the onset of the dry season (JJA) from ~4.0 to ~3.0 g/cm^2. However, the influence of forest evapotranspiration contributes for moisture maintenance in the later of the dry season (Costa et al., 2010; Harper et al., 2014). Wright et al. (2017) found a strong signal that rainforest induces the wet season onset over southern Amazon, and our results present an increase of CWV content around October and November over the AMZ4 region. In addition to seasonal variability, Fig. 7c shows a significant increasing trend of Δδ CWV over all regions between 2012 and 2015, and the interannual variability of Δδ CWV is more evident in the southern region (AMZ4). In the 2010 drought, southern AMZ4 presented a high variability of water vapor, with $\Delta\delta_{JJA}$ of $-0.4\,g/cm^2$ compared to $\sim 0.1\,g/cm^2$ over the other regions.

4.4. Climate variability: drought and flood effects

Natural climate variability modulates the occurrence of extreme drought and flood episodes in the Amazon basin. As we discussed earlier, anomalous SST modes of equatorial Pacific and tropical Atlantic Oceans induce the extreme episodes, occurring separately or together (Yoon and Zeng, 2010; Deser et al., 2010). This natural climate variability is expected to affect the atmospheric constituents due to irregular rainfall distribution (Arvor et al., 2017), thermal anomalies (Jiménez-Muñoz et al., 2013) and fire disturbance (Aragão et al., 2007). Fig. 8 shows the monthly average of atmospheric constituents under three climate conditions: regular (non-drought or flood), drought and flood years. We selected three years for each climate condition and calculated monthly statistics for the northwestern (AMZ1) and southern (AMZ4). We observed that these regions present distinct response depending on the climate conditions. In the northwestern (AMZ1), the total ozone and AOD values were higher in the drought years than those in the regular and flood. Although the cloud cover does not present an abrupt change, it is possible to observe a slightly decreasing in the dry season. The southern region (AMZ4) shows a rapid increase in the AOD values during the drought years, while other constituents were less affected as shown in Fig. 8. Note that peak AOD records were observed between August and October period, indicating the relevance of this period for fire monitoring. We also found that AOD values have low variability during the summer (DJF) and autumn (MAM) periods for both regions - independently of climate conditions. Moreover, water vapor content is relatively low in the dry season over the southern Amazon, being more critical for the drought years. The interannual variability of total ozone content does not present a direct relation with climate conditions because we observed peak TOZ values for both drought and flood years according to AMZ regions.

Figs. 9 and 10 show the (a) percentage area of the Amazon basin under negative Δδ of cloud cover and positive Δδ of AOD, respectively, and (b) spatial distribution of positive anomalies during 2005, 2010 and 2015 droughts. Note that recent drought had an extreme AOD anomaly occurring toward the end of 2015, unlike in 2005 and 2010, and we represented this during October to December season. Fig. 9 revealed that 2005 and 2010 droughts affected cloud cover mostly in austral winter (JJA) with positive anomalies over 69.5% and 63.6% of total basin in this period. In comparison, the 2015 drought presents the negative anomalies covering 80.9% of the basin in the SON season. These results suggest the spatial difference of drought effects (e.g. irregular rainfall distribution) between these years, leading to prolonged dry season in the 2015. Similar drought-induced effects were observed in the AOD anomalies. While September represents the peak month for AOD during 2005 and 2010, the late burning season during 2015 shifted the AOD peak toward the end of year. During the 2005 and 2010 droughts, the positive AOD anomalies ($\delta > 0.1$) occurred over 39.03% (240.3 million ha) and 27.14% (166 million ha) of total basin in the SON season, respectively. However, the recent 2015 drought occurred towards the end of year and these anomalies were observed over 23.72% (145 million ha) during October through December (OND), with most affected areas over central and eastern regions. Note that transport of fire emissions changes the atmospheric loading over large areas, and it does not represent an indication of burned area. While 2015 drought was suggested as the most severe during the last two decades (Jiménez-Muñoz et al., 2016), the percentage of the area under high AOD anomalies (> 0.1) was slightly lower than those of 2005 and 2010 drought (Fig. 12). Since high AOD records in the Amazon basin are at least in part a response to fire emissions, these results represent a positive measure for September records, but we observed that it still affecting the air quality during drought years – these effects extend over regions barely affected in the past.

4.5. Implication for optical remote sensing

Fig. 11 presents the scattering and absorption effects affecting the standard green vegetation spectrum during dry and wet conditions. Satellite sensors and their spectral bands are located in the top panel (Fig. 13a) and the input parameters used in the 6SV model are

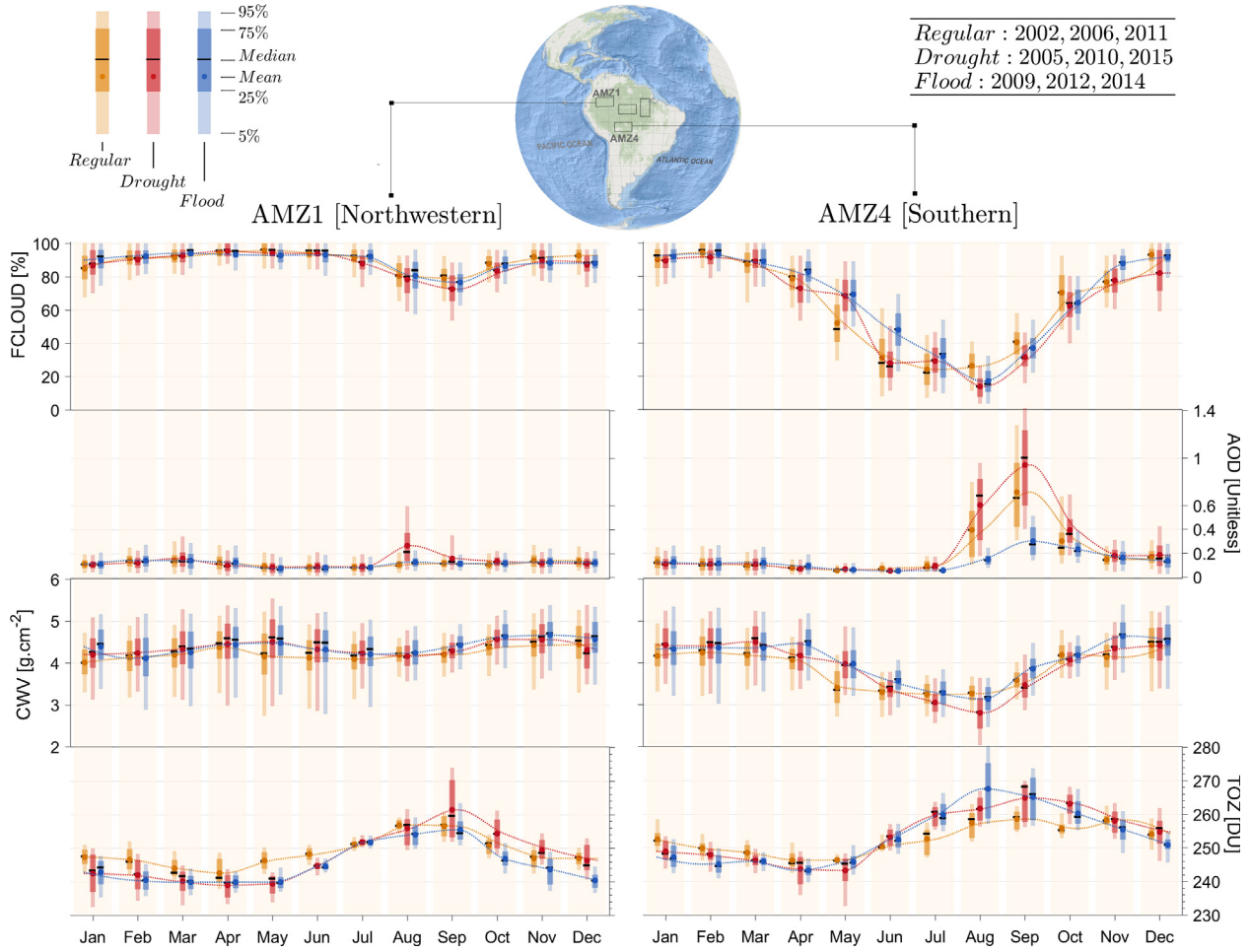

Fig. 8. Monthly variability of atmospheric constituents for regular, drought and flood years. In each climate condition, the mean and standard deviation was calculated using 300.000 random values (100.000 per year) from northwestern and southern regions.

described for each atmospheric condition in the middle-right table. The simulation applies an atmospheric loading from (b) southern Amazon (AMZ4) in September 2007 and (c) northwestern Amazon (AMZ1) in November 2014. In the visible portion, scattering effects show an exponential decay with increasing wavelengths. The aerosol burden is most severe in blue and green bands and scattering increases the reflectance at 500 nm about 94.78% in dry conditions. Our findings illustrate that aerosol and Rayleigh scattering lead to main bias in the visible spectrum during dry conditions, while molecular scattering is the most additive effect in the wet condition due to low aerosol burden (AOD: 0.11). It is worth noting that low AOD (0.01–0.2) is the most frequent loading in Amazon (Figs. 5 and 6), and our results show a small additive aerosol effect under this range – although aerosol scattering varies with other factors, such as aerosol type, elevation, and sun-view geometry. Therefore, because AOD is seasonally dependent, remote sensing users benefit of the knowledge on cloud-free periods under low aerosol loading to minimize distortions in the TOA measurements. For instance, the cloud cover fraction is nearly the same in July and August over the most part of Amazon basin, but the AOD records are extremely different (Fig. 12). The users should consider the available images from July (AOD: 0.1–0.2) than those of August (AOD: 0.2–0.6) when possible.

While additive effects have affected the visible portion, water vapor presents strong absorption features in the near-infrared spectrum. Due to abundant water vapor in the Amazon basin, the sensitivity analysis shows quite similar attenuation in both dry (3.08 g/cm^2) and wet (4.88 g/cm^2) conditions followed by impacts on the transmittance at 0.720; 0.760; 0.810–0.830; 0.910–0.980; 1.10–1.20; and 2.10 µm. However, note that some spectral channels useful for vegetation indices (NDVI, EVI) are under low or no water vapor effects, e.g. NIR bands, such as MODIS and VIIRS at 0.88 µm, and other visible bands. Note that aerosol burden also affects sunlight propagation by diffuse transmittance (upward and downward), which can be easily observed in NIR portion during dry conditions. Therefore, these results suggest that empirical atmospheric correction methods focused on additive effects, such as dark-object subtraction, might be inappropriate for certain remote sensing applications. Regarding the ozone effects, the transmittance decreases in the green (~0.550 µm) and red (0.670 µm) bands, while infrared bands have low or no effect from ozone absorption (T_{O3} = 1.0). Since the distribution of ozone is quite spatially stable across the Amazon basin, this constituent is more "predictable" than aerosol and water vapor, and climatology might be sufficient for some atmospheric correction approaches.

5. Discussion

This study provides a novel assessment of seasonal patterns of atmosphere constituents using new multi-angle MODIS (MAIAC) and standard MOD08 product (2000–2015). Due to the challenges of remote sensing over the Amazon basin, we used the most critical atmospheric constituents in a unique assessment over the basin to support both climate analysis and satellite-based sensing applications. We have shown that cloud cover has a seasonal and regional variation across the Amazon basin (Figs. 5 and S1), imposing a severe limitation for surface observation. For instance, Figs. 5 and 6ci show that the northwestern region presents high and quasi-permanent cloud cover throughout the

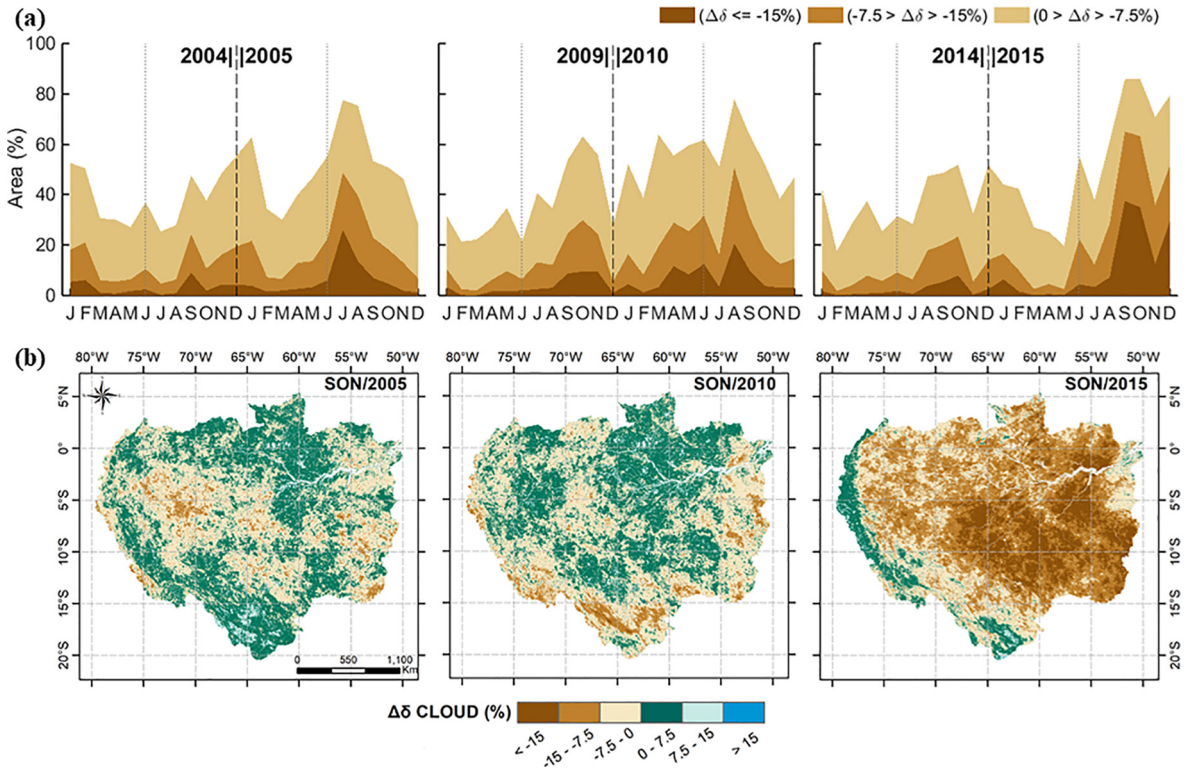

Fig. 9. Temporal patterns of cloud cover on the drought years. (a) Percentage of area of the Amazon basin under negative non-standardized anomalies (Δδ) of cloud cover fraction in 2004–2005, 2009–2010 and 2014–2015. (b) Spatial distribution of negative Δδ of cloud cover in SON 2005, 2010 and 2015.

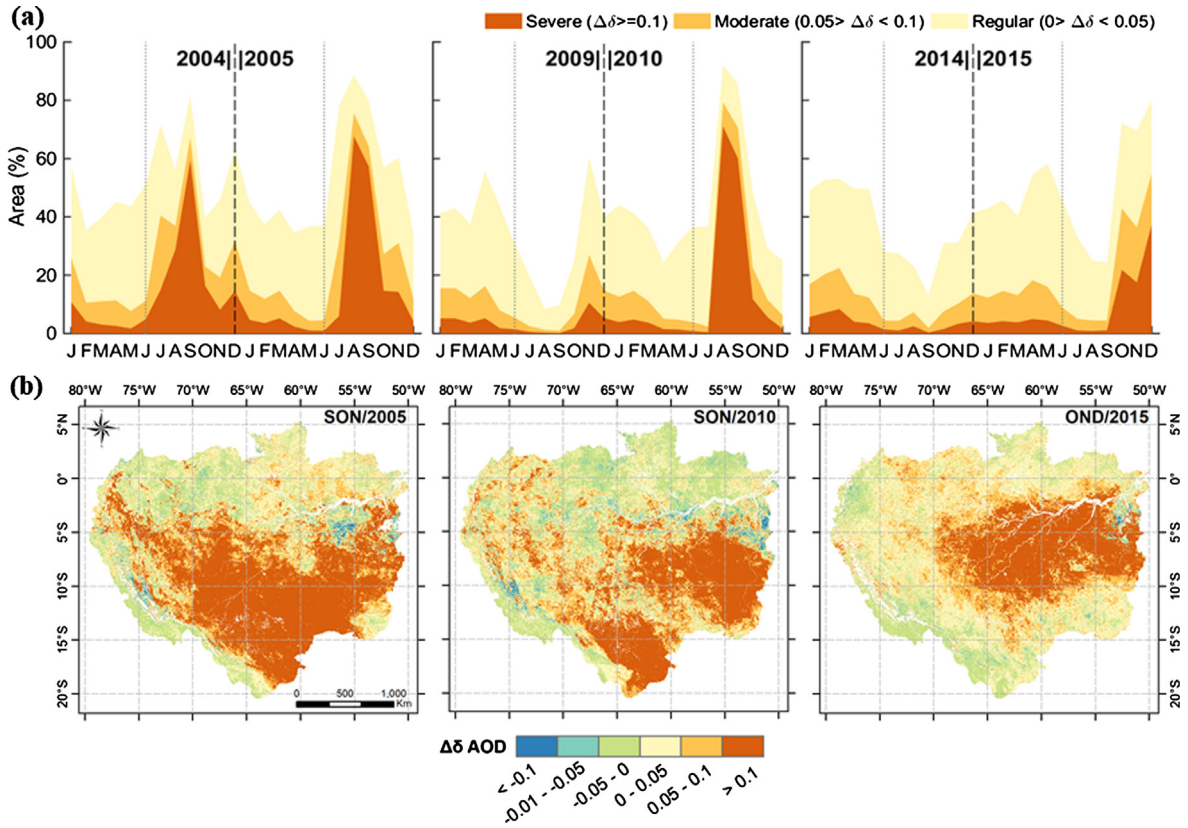

Fig. 10. Temporal patterns of aerosol optical depth (AOD) on the drought years. (a) Percentage of area of the Amazon basin under positive non-standardized anomalies (Δδ) of AOD in 2004–2005, 2009–2010 and 2014–2015. (b) Spatial distribution of positive Δδ of AOD for SON season in 2005, 2010 and for OND season in 2015.

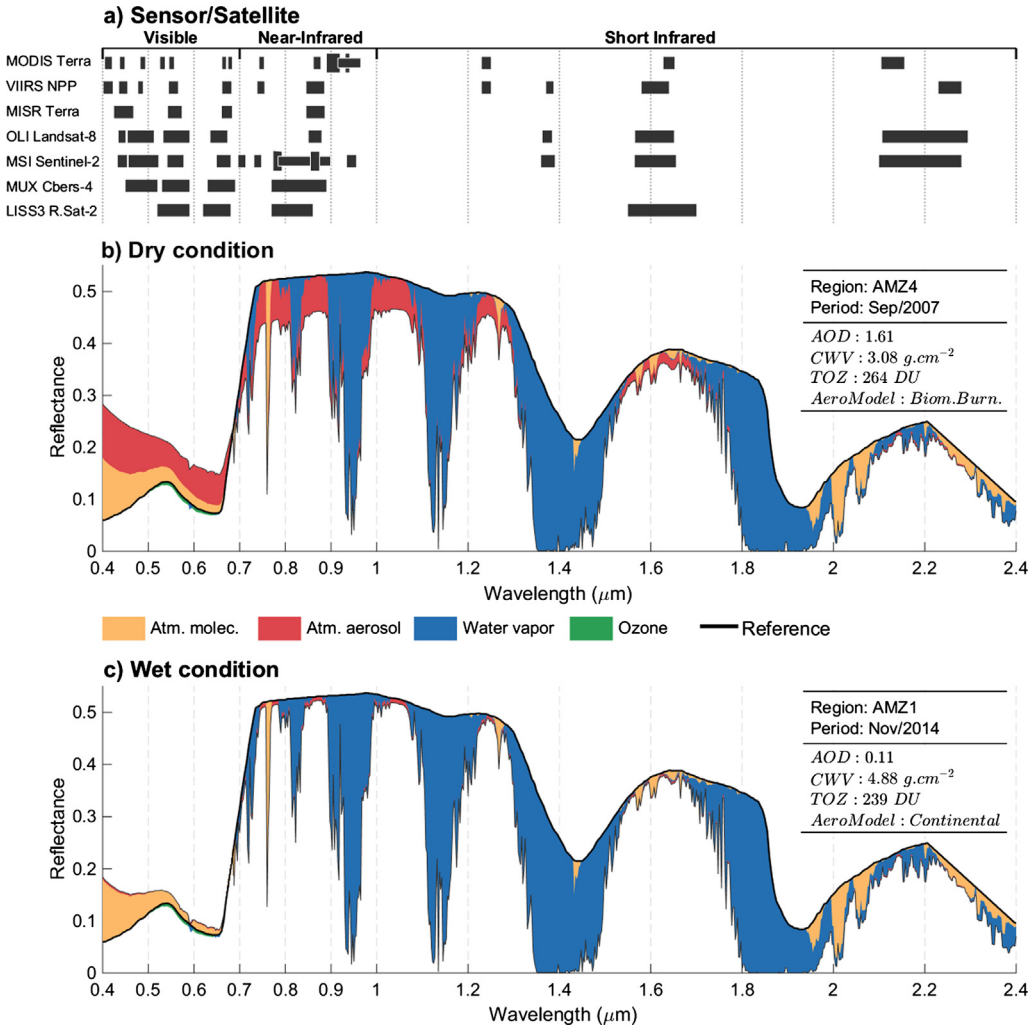

Fig. 11. Simulations of atmospheric scattering and absorption, affecting standard green vegetation spectrum, during dry and wet conditions. (a) Satellite sensors and their spectral bands as user's reference; (b) dry condition in September 2007 over southern Amazon (AMZ4); and (c) wet condition in November 2014 over northwestern Amazon (AMZ1). The model input variables used in the 6SV model are described in the middle-right table. The wavelength is in micrometer (μm). (For interpretation of the references to colour in this figure legend, the reader is referred to the web version of this article.)

year, while the other regions present relative low cloud cover (0–40%) during 3 to 5 months. Note that diurnal variation was not considered in this analysis and the cloud cover varies from morning to afternoon. Our results of cloud cover are consistent in both magnitude and spatio-temporal distribution with previous studies (Asner 2001; Hilker et al., 2012). In addition to this discussion, Fu et al. (2013) reported that changes on the dry season length over southern Amazon may expose this region to prolonged dry period, and consequently, it might influence the cloud cover and burned area in coming decades. Our results presented in Fig. 5 show that when cloud cover reaches the lowest fraction in the southern sub-basins, the aerosol loading increases few months later with values higher than 0.2. This abrupt change in the atmosphere turbidity imposes some challenges for remote sensing in the cloud-free period (Asner and Alencar, 2010). For instance, the aerosol scattering can increase the apparent reflectance of vegetation by three times in the dry condition (Fig. 11). Thus, while low aerosol burden (< 0.2) was observed in the wet season (Figs. 5 and 6, and S2), the biomass burning emissions change drastically the atmospheric turbidity during the late dry season (SON) over the most part of Amazon (Table 2, Figs. 5, 10 and S2).

Landscape fires have been used to land-use conversion, land clearing for cattle ranching and agricultural activities (Aragão et al., 2008; Chen et al., 2013). During this timeline (2000–2015), we have shown that the most critical AOD episodes occurred in the 2005 and 2007 (Fig. 7). Similarly, Aragão and Shimabukuro (2010) reported a fire increase between 1998 and 2007, although annual deforestation rates have reduced after 2004 (Aragão et al., 2014; Reddington et al., 2015). Additionally, Morton et al. (2008) quantified that 84% of fires incidence (2003–2007) was detected in active deforestation frontiers, such as Bolivia and Brazilian states of Mato Grosso, Pará, and Rondônia. Our results show that aerosol loading has a progressive decreasing trend over studied period, especially, in the southern Amazon (Fig. 7). However, the large areas with positive anomalies of AOD ($\Delta\delta > 0.1$) were observed during all three droughts (2005, 2010, 2015). These anomalies present regional effects among the years (Fig. 10). For instance, the 2015 drought has a high AOD records over central and eastern Amazon, while 2005 and 2010 had the most affected regions in the southern and western Amazon. These findings are consistent with spatial distribution of active fire incidence in the Brazilian Amazon (Aragão et al., 2018). These authors also reported that drought-induced fires surpass those of deforestation, with strong evidences of decoupling of fires occurrences from deforestation. In addition, Andela et al. (2017) reported positive burned area trend over central-eastern region, which suggests that human-driven fires are changing from tropical forest frontiers to areas barely affected in the past. Therefore, continuous efforts are needed to maintain positive progress on the air quality across

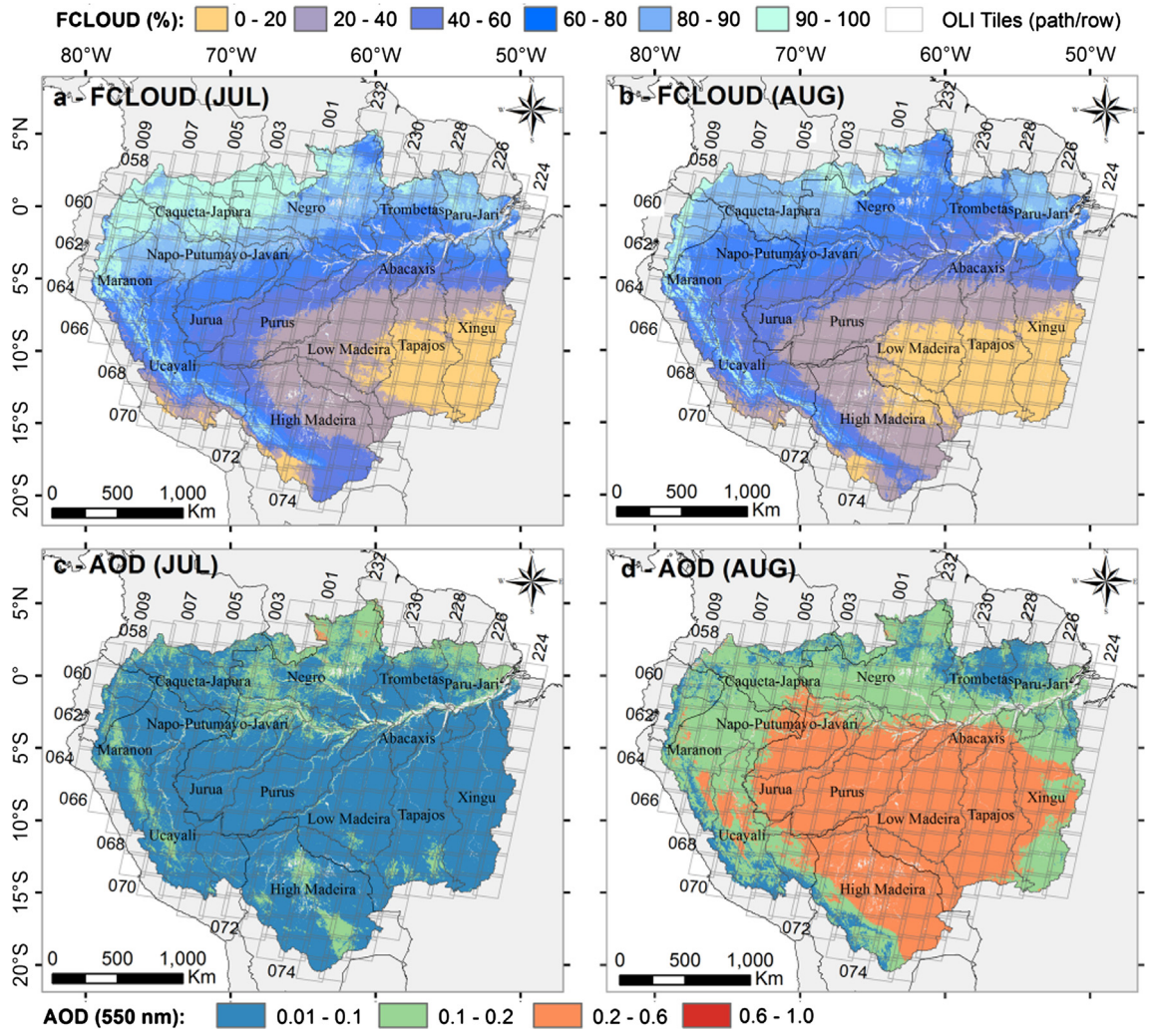

Fig. 12. Spatial distribution of cloud cover fraction (a, b) and aerosol optical depth (c, d) in July and August from averaged data (2000–2015). The Landsat-8 scene grid (path/row) is shown superimposed in the panels as a reference for remote sensing users. These results have shown that cloud cover fraction is near the same between July and August, but background AOD records are clearly distinct.

the Amazon basin followed by new policies and monitoring systems.

Biomass burning and biogenic emissions contribute, at least in part, to increase the concentration of chemical precursors of tropospheric ozone, such as NOx, VOCs, CH_4, and CO (Akagi et al., 2011; Andreae and Merlet, 2001). In the lower troposphere, the ozone production occurs when precursor emissions and climate factors (sunlight and temperature) are available for photochemical reactions (Royal Society, 2008). Our results show that total ozone content typically ranges between 220 and 270 DU across the Amazon, with seasonal change from 225 to 255 during MAM to 255–270 DU during SON season (Figs. 5 and 6 and S4). Although burning emissions are significant source for tropospheric ozone, this total ozone gradient can also be a result of other factors, such as stratosphere-troposphere exchange, long-range transport of pollutants, lighting NOx and natural VOC emissions (Royal Society, 2008; see Table 6.1). According to Ziemke et al. (2011), the stratospheric ozone has a small variability over the tropics (220–235 DU), while the tropospheric ozone varies within 20 and 40 DU, with maximum in the SON season. These authors also mentioned that this seasonal variation is influenced by both regional emissions and large-scale transport of O_3 from several sources, such as lighting, biomass burning, soil emissions and fossil fuels. Thus, beyond of the O_3 precursors emitted by fire emissions, the lighting NOx and natural VOC emissions also present a significant influence on the ozone concentrations (Karl et al., 2007; Murray et al., 2013). Sauvage et al. (2007) showed from simulations that lightning is the dominant source of ozone in the tropical South Atlantic, which contributes for seasonal tropospheric O_3 variation over the South America. In general, the combination of dynamical and chemical effects leads the seasonal variation of total ozone, and burning emissions are a partial explanation for the regional effects. Due to ozone effects on the air quality and climate, more studies are highly suggested to quantify the impacts of climate-induced change on the tropospheric ozone.

Large-scale atmospheric circulation and local moisture recycling are relevant mechanisms influencing moisture feedback in the tropical rainforest region (Eltahir and Bras, 1994; Van Der Ent et al., 2010). Our results show that the highest water vapor content takes place in the austral summer (DJF) and autumn (MAM) over Amazon basin (Figs. 5 and 6 and S3). Furthermore, the northern sub-basins present the persistent CWV content of $\sim$4.0–5.5 g cm^{-2} throughout the year, while southern sub-basins present a seasonal variability in concentration spanning from 4.0 to 5.5 g/cm^2 to 2.0–3.5 g/cm^2 between first and second halves of the year. In the southern region, changes in water vapor content as evapotranspiration response contribute to dry-wet transition in a late dry season (Fu and Li, 2004). Malhi et al. (2002) quantified energy and water dynamic using measurements from September 1995 to August 1996 and reported that annual

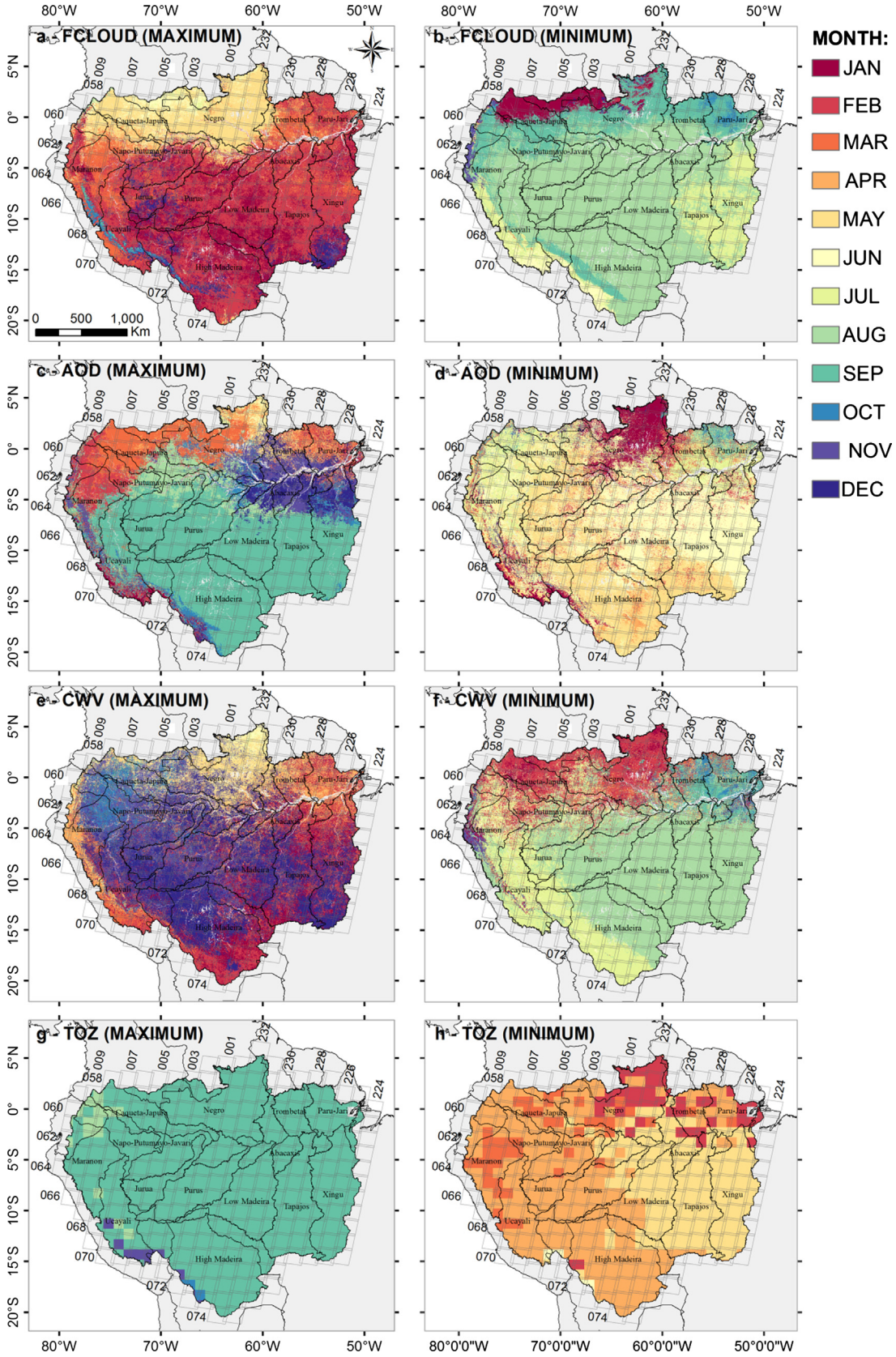

Fig. 13. Maximum and minimum months of (a, b) cloud cover and key atmospheric constituents: (c, d) aerosol optical depth, AOD; (e, f) columnar water vapor, CWV; and (g, h) total columnar ozone, TOZ. The Landsat-8 scene grid (path/row) is used as reference for remote sensing users.

evapotranspiration (1123 mm) contributes with 54% of the rainfall in central Amazon, close to Manaus city. Since the evapotranspiration plays a significant role for maintaining the atmospheric moisture (see references in Marengo, 2006), Amazonian deforestation in the past three decades (Hansen et al., 2013) is expected to cause a reduction in evapotranspiration and so induce changes in moisture budget (Sampaio et al., 2007). However, our results in Fig. 7c show a slight upward trend of CWV records between 2000 and 2015 (~ 0.3 g/cm^2). Recently, some studies found a similar positive trend of water content (Bordi et al.,2014; Gloor et al., 2015). The latter reported an increased moisture transport across Atlantic coast as influence of tropical Atlantic surface warming. Although these studies present strong evidences of moisture exchange, we also suggest that high temperatures may increase the evapotranspiration on the short-term, but it can change (and decrease) at long-term due to rainforest response to water and thermal stress (Nobre and Borma, 2009b). In this sense, additional analysis of radiosonde dataset can be useful to clarify the long-term changes in the meteorological parameters, such as pressure, temperature, water vapor and relative humidity (Sobrino et al., 2015).

We have shown that some atmospheric constituents are fairly constant over a short period, such as water vapor and ozone (Figs. 5 and 6), and the climatology information might be sufficient when atmospheric properties are not available or coincident with satellite overpass. When fine-resolution sensors do not provide useful channels to retrieve atmospheric properties, an alternative approach must be applied to account for atmospheric correction. For instance, Zelazowski et al. (2011) explored the reconciliation of moderate-resolution atmospheric products as an alternative input variable for atmospheric correction of Landsat ETM+ over high and low altitudes in the Peruvian Amazon. In turn, aerosols present a rapid change in the atmosphere column and strong scattering effects in the visible portion of the spectrum, which makes this constituent a great challenge for the remote sensing applications.

Recent studies reported that undetected cloud and aerosol effects often induce an inaccurate interpretation of vegetation response during drought years (Hilker et al., 2012; Samanta et al., 2010, Asner and Alencar, 2010), and our results show how critical and variable is the aerosol loading between seasons, and especially in extreme climate years (Fig. 10). Particularly, Hilker et al. (2012) assessed the uncertainties in MODIS surface reflectance products (e.g. MAIAC, MYD09, MYD09GA and derived composites) to characterize the Amazon's vegetation dynamics and they emphasized the residual cloud and aerosol contamination in the vegetation indices. So, it seems relevant that remote sensing users might consider the seasonal pattern of constituents to minimize the atmospheric bias in the satellite-derived data. Thus, Fig. 13 illustrates the extreme months (max. and min.) for each constituent to help the users in the understanding of the reference dates (highest versus lowest concentrations). For instance, it should be noted that while minimum cloud cover occurs in July and August, the lower AOD loading and ozone is 1–2 months early (May-June). Furthermore, in terms of remote sensing, the minimum cloud cover also happens under the low CWV content. We hope that these maximum and minimum statistics can be useful to define better clear-sky periods or to support the design of field experiments.

6. Summary and conclusion

In this paper, we provide a long-term assessment of cloud cover fraction and atmospheric constituents using 15-years MODIS-MAIAC data (2000–2015) across Amazon basin. The validation of AOD and CWV shows a fair agreement of MAIAC retrievals and AERONET measurements ($R > 0.81$). The seasonal and interannual variability of atmospheric constituents imposes several challenges for remote sensing applications in the Amazon basin. Our findings show that northwestern Amazon presents a persistent cloudy condition (60 to 100%) over the 10-month period. During the austral winter (JJA) and spring (SON) season, the cloud cover fraction decays to 10–40% in most part of the Amazon, which represents an outstanding period for cloud-free images. We also observed that aerosol burden is highly heterogeneous and changes rapidly in the dry season (AOD > 0.2). Moreover, AOD records are relatively sensitive to drought years as consequence of fire occurrences, and record-loading values are clearly observed during the 2005 and 2007 drought when $\Delta\delta_{SON}$ AOD exceeds 0.25. But, a positive measure was observed for long-term aerosol loading across the Amazon basin due to decreasing AOD values in the all studied areas. Although this decreasing AOD trend represents a positive result for air quality, the drought years are still changing the aerosol loading during burning season.

We observed high concentration values for the water vapor across the Amazon, ranging from 3.0 to 5.0 g/cm^2, except over Andes Mountains. In the regional analysis, the highest water vapor was found in the northwestern and central Amazon (~ 4.5 g/cm^2), while the other regions showed a high seasonal variability throughout the year (variation of ~ 2.0 g/cm^2). It should be noted that water vapor presents a slight upward trend within 2000–2015. Further analysis should be conducted to clarify the reasons of this apparent climate signal. Our results show a relative low total O_3 during first half of the year (~ 245 DU) and increase 5.7% toward the end of the year (260 DU). Although total ozone content is relatively constant than other constituents, we found a positive anomalies of total ozone ($\Delta\delta_{SON} > 20$ DU) during 2015 drought followed by negative $\Delta\delta_{SON}$ of cloud cover values.

In the last decades, Amazon basin has experienced intense land-use change harboring several long-term environmental impacts: damming the rivers, forest fires, loss of protected areas, expansion of mining industry, and intensification of agribusiness (Nobre et al., 2016; Nepstad et al., 2014; Latrubesse et al., 2017; Lobo et al., 2016; Soares-Filho et al., 2006; Arvor et al., 2018). In this sense, continuous efforts are needed for future monitoring and conservation, what makes remote sensing tools useful for several purposes in this region but rather dependent on the satellite design, image processing and sampling techniques (e.g. Eva et al., 2010; Lu et al., 2016). Due to high cloud cover condition, near-daily MODIS/Terra and VIIRS/Suomi-NPP observations and harmonization of MSI/Sentinel-2 and OLI-Landsat-8 dataset can increase the probability of cloud-free observations. Furthermore, the upcoming Amazonia-1 satellite, carrying optical Wide Field Imager (WFI), will provide useful multi-spectral data covering wide swath (~ 780 km) with 5-day revisit at 40 m spatial resolution. Although those polar orbit satellite sensors increase the opening and valuable data for Amazon studies, the rigorous atmospheric correction and cloud detection remain a challenge for high-quality surface products. Additionally, the geostationary satellites become a potential data source at coarse spatial resolution, but it also demands an extensive research effort regarding on atmospheric correction. Finally, this study contributes to the long-term analysis of atmospheric constituents, linking their patterns with remote sensing applications across the Amazon basin.

Acknowledgements

We gratefully acknowledge the NASA and MODIS team for the maintenance of satellite atmospheric products. We also thank AERONET PIs (Dr. Brent Holben and Dr. Paulo Artaxo) for providing sun photometer data. The MAIAC and MOD08 products are available at ftp://dataportal.nccs.nasa.gov/DataRelease/SouthAmerica/ and ftp://ladsweb.nascom.nasa.gov/allData/6/MOD08_D3/, respectively. Luiz E.O.C. Aragao thanks the Brazilian National Research Council (CNPQ – 305054/2016-3). We thank Lino S. Carvalho and Hilton Ferraz for valuable comments in the analysis. We also thank Dr. Robin Wilson for providing Py6S (Python interface to 6SV) with full description (Wilson, 2013). The climatology products derived from this study are available at http://www.dpi.inpe.br/atmc/. We thank four anonymous reviewers for their insightful comments.

Appendix A. Supplementary material

Supplementary data associated with this article can be found, in the online version, at https://doi.org/10.1016/j.isprsjprs.2018.05.013.

References

Akagi, S.K., Yokelson, R.J., Wiedinmyer, C., Alvarado, M.J., Reid, J.S., Karl, T., Crounse, J.D., Wennberg, P.O., 2011. Emission factors for open and domestic biomass burning for use in atmospheric models. Atmos. Chem. Phys. 11 (9), 4039–4072. http://dx.doi.org/10.5194/acp-11-4039-2011.

Aguiar, D.A., Mello, M.P., Nogueira, S.F., Gonçalves, F.G., Adami, M., Rudorff, B.F.T., 2017. MODIS time series to detect anthropogenic interventions and degradation processes in tropical pasture. Remote Sensing 9 (1), 73.

Andela, N., Morton, D.C., Giglio, L., Chen, Y., van der Werf, G.R., Kasibhatla, P.S., DeFries, R.S., Collatz, G.J., Hantson, S., Kloster, S., Bachelet, D., Forrest, M., Lasslop, G., Li, F., Mangen, S., Melton, J.R., Yue, C., Randerson, J.T., 2017. A human-driven decline in global burned area. Science 356 (6345), 1356–1362.

Anderson, L.O., Malhi, Y., Aragão, L.E., Ladle, R., Arai, E., Barbier, N., Phillips, O., 2010. Remote sensing detection of droughts in Amazonian forest canopies. New Phytol. 187 (3), 733–750.

Andreae, M.O., Merlet, P., 2001. Emission of trace gases and aerosols from biomass burning. Global Biogeochem. Cycles 15 (4), 955–966.

Aragão, L.E.O., Malhi, Y., Roman-Cuesta, R.M., Saatchi, S., Anderson, L.O., Shimabukuro, Y.E., 2007. Spatial patterns and fire response of recent Amazonian droughts. Geophys. Res. Lett. 34 (7).

Aragão, L.E.O.C., Malhi, Y., Barbier, N., Lima, A.A., Shimabukuro, Y., Anderson, L., Saatchi, S., 2008. Interactions between rainfall, deforestation and fires during recent years in the Brazilian Amazonia. Philos. Trans. R. Soc. Lond. Series B, Biological Sciences 363 (1498), 1779–1785. http://dx.doi.org/10.1098/rstb.2007.0026.

Aragão, L.E.O.C., Shimabukuro, Y.E., 2010. The incidence of fire in Amazonian forests with implications for REDD. Science 328 (5983), 1275–1278. http://dx.doi.org/10.1126/science.1186925.

Aragão, L.E.O.C., Poulter, B., Barlow, J.B., Anderson, L.O., Malhi, Y., Saatchi, S., Gloor, E., 2014. Environmental change and the carbon balance of Amazonian forests. Biol. Rev. 89 (4), 913–931. http://dx.doi.org/10.1111/brv.12088.

Aragão, L.E., Anderson, L.O., Fonseca, M.G., Rosan, T.M., Vedovato, L.B., Wagner, F.H., Barlow, J., 2018. 21st Century drought-related fires counteract the decline of Amazon deforestation carbon emissions. Nature Commun. 9 (1), 536.

Arantes, A.E., Ferreira, L.G., Coe, M.T., 2016. The seasonal carbon and water balances of the Cerrado environment of Brazil: Past, present, and future influences of land cover and land use. ISPRS J. Photogramm. Remote Sens. 117, 66–78.

Artaxo, P., Rizzo, L.V., Brito, J.F., Barbosa, H.M.J., Arana, A., Sena, E.T., Cirino, G.C., Bastos, W., Martin, S.T., Andreae, M.O., 2013. Atmospheric aerosols in Amazonia and land use change: from natural biogenic to biomass burning conditions. Faraday Discuss. 165, 203. http://dx.doi.org/10.1039/c3fd00052d.

Arvor, D., Meirelles, M., Dubreuil, V., Begue, A., Shimabukuro, Y.E., 2012. Analyzing the agricultural transition in Mato Grosso, Brazil, using satellite-derived indices. Appl. Geogr. 32 (2), 702–713.

Arvor, D., Funatsu, B.M., Michot, V., Dubreuil, V., 2017. Monitoring rainfall patterns in the southern Amazon with PERSIANN-CDR Data: long-term characteristics and trends. Remote Sensing 9 (9), 889.

Arvor, D., Daher, F.R., Briand, D., Dufour, S., Rollet, A.J., Simões, M., Ferraz, R.P., 2018. Monitoring thirty years of small water reservoirs proliferation in the southern Brazilian Amazon with Landsat time series. ISPRS J. Photogramm. Remote Sens.

Asner, G.P., 2001. Cloud cover in Landsat observations of the Brazilian Amazon. Int. J. Remote Sens. 22 (18), 3855–3862. http://dx.doi.org/10.1080/01431160010006926.

Asner, G.P., Alencar, A., 2010. Drought impacts on the Amazon forest: the remote sensing perspective. New Phytol. 187 (3), 569–578.

Baccini, A., Goetz, S.J., Walker, W.S., Laporte, N.T., Sun, M., Sulla-Menashe, D., Houghton, R.A., 2012. Estimated carbon dioxide emissions from tropical deforestation improved by carbon-density maps. Nature Climate Change 2 (3), 182–185. http://dx.doi.org/10.1038/nclimate1354.

Barbosa, C.C.A., Atkinson, P.M., Dearing, J.A., 2015. Remote sensing of ecosystem services: A systematic review. Ecol. Ind. 52, 430–443. http://dx.doi.org/10.1016/j.ecolind.2015.01.007.

Bevan, S.L., North, P.R., Grey, W.M., Los, S.O., Plummer, S.E., 2009. Impact of atmospheric aerosol from biomass burning on Amazon dry-season drought. J. Geophys. Res.: Atmospheres 114 (D9).

Boers, N., Marwan, N., Barbosa, H. M. J., Kurths, J., 2017. A deforestation-induced tipping point for the South American monsoon system. Scientific Reports, 7(August 2016), 41489. http://doi.org/10.1038/srep41489.

Borbas, E.E., Seemann, S.W., Kern, A.N.I.K.O., Moy, L.E.S.L.I.E., Li, J., Gumley, L.I.A.M., Menzel, W.P., 2011. MODIS atmospheric profile retrieval algorithm theoretical basis document. Electronic resource], http://modis-atmos. GSFC. NASA. gov/MOD07_L2/atbd.

Bordi, I., De Bonis, R., Fraedrich, K., Sutera, A., 2014. Interannual variability patterns of the world's total column water content: Amazon River basin. Theor. Appl. Climatol. 122 (3–4), 441–455. http://dx.doi.org/10.1007/s00704-014-1304-y.

Brando, P.M., Goetz, S.J., Baccini, A., Nepstad, D.C., Beck, P.S., Christman, M.C., 2010. Seasonal and interannual variability of climate and vegetation indices across the Amazon. Proc. Natl. Acad. Sci. 107 (33), 14685–14690.

Carvalho, L.M.V., Jones, C., Liebmann, B., 2004. The South Atlantic convergence zone: Intensity, form, persistence, and relationships with intraseasonal to interannual activity and extreme rainfall. J. Clim. 17 (1), 88–108. http://dx.doi.org/10.1175/1520-0442 (2004)017<0088:TSACZI>2.0.CO;2.

Chambers, J.Q., Asner, G.P., Morton, D.C., Anderson, L.O., Saatchi, S.S., Espírito-Santo, F.D.B., Souza, C., 2007. Regional ecosystem structure and function: ecological insights from remote sensing of tropical forests. Trends Ecol. Evol. 22 (8), 414–423. http://dx.doi.org/10.1016/j.tree.2007.05.001.

Chen, Y., Morton, D.C., Jin, Y., Collatz, G.J., Kasibhatla, P.S., van der Werf, G.R., DeFries, R.S., Randerson, J.T., 2013. Long-term trends and interannual variability of forest, savanna and agricultural fires in South America. Carbon Manage. 4 (6), 617–638. http://dx.doi.org/10.4155/cmt.13.61.

Costa, M.H., Biajoli, M.C., Sanches, L., Malhado, A.C.M., Hutyra, L.R., Da Rocha, H.R., Aguiar, R.G., Araujo, A.C., 2010. Atmospheric versus vegetation controls of Amazonian tropical rain forest evapotranspiration: Are the wet and seasonally dry rain forests any different? J. Geophys. Res. Biogeosci. 115 (4), 1–9. http://dx.doi.org/10.1029/2009JG001179.

Cox, P.M., Harris, P.P., Huntingford, C., Betts, R.A., Collins, M., Jones, C.D., Nobre, C.A., 2008. Increasing risk of Amazonian drought due to decreasing aerosol pollution. Nature 453 (7192), 212.

Davidson, E.A., de Araújo, A.C., Artaxo, P., Balch, J.K., Brown, I.F., C. Bustamante, M.M., Wofsy, S.C., 2012. The Amazon basin in transition. Nature, 481(7381), 321–328. http://doi.org/10.1038/nature10717.

Deser, C., Alexander, M.A., Xie, S.P., Phillips, A.S., 2010. Sea surface temperature variability: Patterns and mechanisms. Ann. Rev. Marine Sci. 2, 115–143.

Doughty, C.E., Metcalfe, D.B., Girardin, C.A.J., Amézquita, F.F., Cabrera, D.G., Huasco, W.H., Feldpausch, T.R., 2015. Drought impact on forest carbon dynamics and fluxes in Amazonia. Nature 519 (7541), 78.

Eck, T.F., Holben, B.N., Reid, J.S., Dubovik, O., Smirnov, A., O'Neill, N.T., Slutsker, I., Kinne, S., 1999. Wavelength dependence of the optical depth of biomass burning, urban, and desert dust aerosols. J. Geophys. Res. D: Atmos. 104 (1), 31333–31349. http://dx.doi.org/10.1029/1999JD900923.

Eltahir, E.A.B., Bras, R.L., 1994. Precipitation recycling in the Amazon basin. Q. J. R. Meteorolog. Soc. 120 (518), 861–880. http://dx.doi.org/10.1002/qj.49712051806.

Emck, P., 2007. A Climatology of South Ecuador-with special focus on the Major Andean Ridge as Atlantic-Pacific Climate Divide.

Eva, H., Carboni, S., Achard, F., Stach, N., Durieux, L., Faure, J.F., Mollicone, D., 2010. Monitoring forest areas from continental to territorial levels using a sample of medium spatial resolution satellite imagery. ISPRS J. Photogramm. Remote Sens. 65 (2), 191–197.

Feng, M., Sexton, J.O., Huang, C., Masek, J.G., Vermote, E.F., Gao, F., Townshend, J.R., 2013. Global surface reflectance products from Landsat: Assessment using coincident MODIS observations. Remote Sens. Environ. 134, 276–293. http://dx.doi.org/10.1016/j.rse.2013.02.031.

Fioletov, V.E., 2008. Ozone climatology, trends, and substances that control ozone. Atmos. Ocean 46 (1), 39–67.

Freitas, S.R., Longo, K.M., Dias, M.A.S., Dias, P.L.S., Chatfield, R., Prins, E., Recuero, F.S., 2005. Monitoring the transport of biomass burning emissions in South America. Environ. Fluid Mech. 5 (1–2), 135–167.

Fu, R., Dickinson, R., Chen, M., Wang, H., 2001. How do tropical sea surface temperatures influence the seasonal distribution of precipitation in the equatorial Amazon? J. Climate, (Gibbs 1979), 4003–4026.

Fu, R., Li, W., 2004. The influence of the land surface on the transition from dry to wet season in Amazonia. Theor. Appl. Climatol. 78 (1–3), 97–110. http://dx.doi.org/10.1007/s00704-004-0046-7.

Fu, R., Yin, L., Li, W., Arias, P.A., Dickinson, R.E., Huang, L., Myneni, R.B., 2013. Increased dry-season length over southern Amazonia in recent decades and its implication for future climate projection. Proc. Natl. Acad. Sci. 110 (45), 18110–18115.

Gao, B.C., Montes, M.J., Davis, C.O., Goetz, A.F., 2009. Atmospheric correction algorithms for hyperspectral remote sensing data of land and ocean. Remote Sens. Environ. 113, S17–S24.

Garreaud, R.D., 2009. The Andes climate and weather. Adv. Geosci. 22, 3–11. http://dx.doi.org/10.5194/adgeo-22-3-2009.

Grimm, A.M., Tedeschi, R.G., 2009. ENSO and extreme rainfall events in South America. J. Clim. 22 (7), 1589–1609. http://dx.doi.org/10.1175/2008JCLI2429.1.

Grimm, A.M., 2011. Interannual climate variability in South America: impacts on seasonal precipitation, extreme events, and possible effects of climate change. Stoch. Env. Res. Risk Assess. 25 (4), 537–554. http://dx.doi.org/10.1007/s00477-010-0420-1.

Gloor, M., Barichivich, J., Ziv, G., Brienen, R., Schöngart, J., Peylin, P., Baker, J., 2015. Recent Amazon climate as background for possible ongoing and future changes of Amazon humid forests. Global Biogeochem. Cycles 29 (9), 1384–1399.

Grodsky, S.A., Carton, J.A., 2003. The intertropical convergence zone in the South Atlantic and the equatorial cold tongue. J. Clim. 16 (4), 723–733. http://dx.doi.org/10.1175/1520-0442(2003)016<0723:TICZIT>2.0.CO;2.

Hansen, M.C., Potapov, P.V., Moore, R., Hancher, M., Turubanova, S.A., Tyukavina, A., Thau, D., Stehman, S.V., Goetz, S.J., Loveland, T.R., Kommareddy, A., Egorov, A., Chini, L., Justice, C.O., Townshend, J.R.G., 2013. High-Resolution Global Maps of 21st-Century Forest Cover Change. Science 342 (6160), 850–853. http://dx.doi.org/10.1126/science.1244693.

Harper, A., Baker, I.T., Denning, A.S., Randall, D.A., Dazlich, D., Branson, M., 2014. Impact of evapotranspiration on dry season climate in the Amazon forest. J. Clim. 27 (2), 574–591. http://dx.doi.org/10.1175/JCLI-D-13-00074.1.

Hilker, T., Lyapustin, A.I., Tucker, C.J., Sellers, P.J., Hall, F.G., Wang, Y., 2012. Remote sensing of tropical ecosystems: Atmospheric correction and cloud masking matter. Remote Sens. Environ. 127, 370–384. http://dx.doi.org/10.1016/j.rse.2012.08.035.

Hilker, T., Lyapustin, A.I., Tucker, C.J., Hall, F.G., Myneni, R.B., Wang, Y., Sellers, P.J., 2014. Vegetation dynamics and rainfall sensitivity of the Amazon. Proc. Natl. Acad.

Sci. 111 (45), 16041–16046.
Hilker, T., Lyapustin, A.I., Hall, F.G., Myneni, R., Knyazikhin, Y., Wang, Y., Bi, J., Moura, Y.M., Sellers, P.J., 2015. On the measurability of change in Amazon vegetation from MODIS. Remote Sens. Environ. 166, 233–242. http://dx.doi.org/10.1016/j.rse.2015.05.020.
Hoelzemann, J.J., Longo, K.M., Fonseca, R.M., Do Rosário, N.M.E., Eibern, H., Freitas, S.R., Pires, C., 2009. Regional representative of AERONET observation sites during the biomass burning season in South America determined by correlation studies with MODIS Aerosol Optical Depth. J. Geophys. Res. Atmospheres 114 (13), 1–20. http://dx.doi.org/10.1029/2008JD010369.
Holben, B.N., Eck, T.F., Slutsker, I., Tanré, D., Buis, J.P., Setzer, A., Vermote, E., Reagon, J.A., Kaufman, Y.J., Nakajima, T., Lavenu, F., Jankowiak, I., Smirnov, A., 1998. AERONET—A federated instrument network and data archive for aerosol characterization. Remote Sens. Environ. 66 (1), 1–16. http://dx.doi.org/10.1016/S0034-4257(98)00031-5.
Hubanks, P., Platnick, S., King, M., Ridgway, B., 2015. MODIS Atmosphere L3 Gridded Product Algorithm Theoretical Basis Document (ATBD) & Users Guide, ATBD reference number ATBDMOD-30, NASA, 125 pp.. https://modis-images.gsfc.nasa.gov/_docs/L3_ATBD_C6.pdf.
Huffman, G.J., Bolvin, D.T., Nelkin, E.J., Wolff, D.B., Adler, R.F., Gu, G., Bowman, K., Hong, Y., Stocker, E.F., 2007. The TRMM multisatellite precipitation analysis (TMPA): Quasi-global, multiyear, combined-sensor precipitation estimates at fine scales. J. Hydrometeorol. 8 (1), 38–55.
Ignotti, E., Valente, J.G., Longo, K.M., Freitas, S.R., Hacon, S.D.S., Artaxo Netto, P., 2010. Impact on human health of particulate matter emitted from burnings in the Brazilian Amazon region. Revista de saude publica 44 (1), 121–130.
Jaffe, D.A., Wigder, N.L., 2012. Ozone production from wildfires: A critical review. Atmos. Environ. 51, 1–10. http://dx.doi.org/10.1016/j.atmosenv.2011.11.063.
Jardine, K., Jardine, A., 2016. Biogenic volatile organic compounds in Amazonian forest ecosystems. Between Biosphere, Atmosphere and Human Land Retrieved from http://link.springer.com/chapter/10.1007/978-3-662-49902-3_2.
Jiménez-Muñoz, J.C., Sobrino, J.A., Mattar, C., Malhi, Y., 2013. Spatial and temporal patterns of the recent warming of the Amazon forest. J. Geophys. Res.: Atmospheres 118 (11), 5204–5215.
Jiménez-Muñoz, J.C., Mattar, C., Barichivich, J., Santamaría-Artigas, A., Takahashi, K., Malhi, Y., Sobrino, J.A., van der Schrier, G., 2016. Record-breaking warming and extreme drought in the Amazon rainforest during the course of El Niño 2015–2016. Sci. Rep. 6 (September), 33130. http://dx.doi.org/10.1038/srep33130.
Karl, T., Guenther, A., Yokelson, R.J., Greenberg, J., Potosnak, M., Blake, D.R., Artaxo, P., 2007. The tropical forest and fire emissions experiment: Emission, chemistry, and transport of biogenic volatile organic compounds in the lower atmosphere over Amazonia. J. Geophys. Res. Atmospheres 112 (18), 1–17. http://dx.doi.org/10.1029/2006JD008539.
Koren, I., Remer, L.A., Kaufman, Y.J., Rudich, Y., Martins, J.V., 2007. On the twilight zone between clouds and aerosols. Geophys. Res. Lett. 34 (8), 1–5. http://dx.doi.org/10.1029/2007GL029253.
Latrubesse, E.M., Arima, E.Y., Dunne, T., Park, E., Baker, V.R., d'Horta, F.M., Wight, C., Wittmann, F., Zuanon, J., Baker, P.A., Ribas, C.C., Norgaard, R.B., Filizola, N., Ansar, A., Flyvbjerg, B., Stevaux, J.C., 2017. Damming the rivers of the Amazon basin. Nature 546 (7658), 363–369.
Lobo, F.D.L., Costa, M., Novo, E.M.L.D.M., Telmer, K., 2016. Distribution of artisanal and small-scale gold mining in the Tapajós River Basin (Brazilian Amazon) over the past 40 years and relationship with water siltation. Remote Sensing 8 (7), 579.
Lyapustin, A.I., Wang, Y., Frey, R., 2008. An automatic cloud mask algorithm based on time series of MODIS measurements. J. Geophys. Res. Atmospheres 113 (16), 1–15. http://dx.doi.org/10.1029/2007JD009641.
Lyapustin, A., Martonchik, J., Wang, Y., Laszlo, I., Korkin, S., 2011a. Multi-angle implementation of atmospheric correction (MAIAC): Part 1. Radiative transfer basis and look-up tables. J. Geophys. Res., 116, D03210. http://dx.doi.org/%2010.1029/2010JD014985.
Lyapustin, A., Wang, Y., Laszlo, I., Kahn, R., Korkin, S., Remer, L., Levy, R., Reid, J.S., 2011b. Multi-angle implementation of atmospheric correction (MAIAC): Part 2. Aerosol algorithm. J. Geophys. Res., 116, D03211. http://dx.doi.org/%2010.1029/2010JD014986.
Lyapustin, A., Wang, Y., Hilker, T., Hall, F., Sellers, P., Tucker, J., Korkin, S., 2011c. Multi-Angle Implementation of Atmospheric Correction for MODIS (MAIAC). Part 3: Atmospheric Correction A. Lyapustin, Y. Wang, 1. Laszlo, T. Hilker, F. Hall, P. Sellers,. Remote Sensing of Environment, 9(0), 1–18. http://doi.org/http://dx.doi.org/10.1016/j.rse.2012.09.002.
Lu, D., Li, G., Moran, E., Batistella, M., Freitas, C.C., 2011. Mapping impervious surfaces with the integrated use of Landsat Thematic Mapper and radar data: A case study in an urban–rural landscape in the Brazilian Amazon. ISPRS J. Photogramm. Remote Sens. 66 (6), 798–808.
Lu, M., Pebesma, E., Sanchez, A., Verbesselt, J., 2016. Spatio-temporal change detection from multidimensional arrays: Detecting deforestation from MODIS time series. ISPRS J. Photogramm. Remote Sens. 117, 227–236.
Maeda, E.E., Heiskanen, J., Aragão, L.E., Rinne, J., 2014. Can MODIS EVI monitor ecosystem productivity in the Amazon rainforest? Geophys. Res. Lett. 41 (20), 7176–7183.
Maeda, E.E., Galvão, L.S., 2015. Sun-sensor geometry effects on vegetation index anomalies in the Amazon rainforest. GISci. Remote Sensing 52 (3), 332–343.
Malhi, Y., Pegoraro, E., Nobre, A.D., Pereira, M.G.P., Grace, J., Culf, A.D., Clement, R., 2002. Energy and water dynamics of a central Amazonian rain forest. J. Geophys. Res. Atmospheres 107 (20), 1–17. http://dx.doi.org/10.1029/2001JD000623.
Malhi, Y., Roberts, J.T., Betts, R.A., Killeen, T.J., Li, W., Nobre, C.A., 2008. Climate change, deforestation, and the fate of the Amazon. Science (New York, N.Y.) 319 (5860), 169–172. http://dx.doi.org/10.1126/science.1146961.
Marengo, J.A., 2006. On the hydrological cycle of the amazon basin: a historical review and current state-of-the-art. Revista Brasileira de Meteorologia 21 (3), 1–19.
Marengo, J.A., Nobre, C.A., Tomasella, J., Oyama, M.D., de Oliveira, G.S., de Oliveira, R., Camargo, H., Alves, L.M., Brown, I.F., 2008. The drought of Amazonia in 2005. J. Clim. 21 (3), 495–516. http://dx.doi.org/10.1175/2007JCLI1600.1.
Marengo, J.A., Espinoza, J.C., 2016. Extreme seasonal droughts and floods in Amazonia: Causes, trends and impacts. Int. J. Climatol. 36 (3), 1033–1050. http://dx.doi.org/10.1002/joc.4420.
Marshak, A., Wen, G., Coakley Jr., J.A., Remer, L.A., Loeb, N.G., Cahalan, R.F., 2008. A simple model for the cloud adjacency effect and the apparent bluing of aerosols near clouds. J. Geophys. Res., 113(D14), D14S17. http://doi.org/10.1029/2007JD009196.
Martins, V.S., Barbosa, C.C.F., de Carvalho, L.A.S., Jorge, D.S.F., Lobo, F.D.L., Novo, E.M.L.D.M., 2017a. Assessment of atmospheric correction methods for sentinel-2 MSI images applied to amazon floodplain lakes. Remote Sensing 9 (4), 322.
Martins, V.S., Lyapustin, A., Carvalho, L.A.S., Barbosa, C.C.F., Novo, E.M.L.M., 2017b. Validation of high-resolution MAIAC aerosol product over South America. J. Geophys. Res.: Atmospheres.
Morton, D.C., Defries, R.S., Randerson, J.T., Giglio, L., Schroeder, W., van der Werf, G.R., 2008. Agricultural intensification increases deforestation fire activity in Amazonia. Glob. Change Biol. 14 (10), 2262–2275. http://dx.doi.org/10.1111/j.1365-2486.2008.01652.x.
Morton, D.C., Nagol, J., Carabajal, C.C., Rosette, J., Palace, M., Cook, B.D., North, P.R., 2014. Amazon forests maintain consistent canopy structure and greenness during the dry season. Nature 506 (7487), 221–224.
Moura, Y.M., Galvao, L.S., dos Santos, J.R., Roberts, D.A., Breunig, F.M., 2012. Use of MISR/Terra data to study intra-and inter-annual EVI variations in the dry season of tropical forest. Remote Sens. Environ. 127, 260–270.
Moura, Y.M., Galvão, L.S., Hilker, T., Wu, J., Saleska, S., do Amaral, C.H, et al., 2017. Spectral analysis of amazon canopy phenology during the dry season using a tower hyperspectral camera and modis observations. ISPRS J. Photogramm. Remote Sens. 131, 52–64.
Murray, L.T., Logan, J.A., Jacob, D.J., 2013. Interannual variability in tropical tropospheric ozone and OH: The role of lightning. J. Geophys. Res. Atmospheres 118 (19), 11468–11480. http://dx.doi.org/10.1002/jgrd.50857.
Nagol, J.R., Sexton, J.O., Kim, D.H., Anand, A., Morton, D., Vermote, E., Townshend, J.R., 2015. Bidirectional effects in Landsat reflectance estimates: Is there a problem to solve? ISPRS J. Photogramm. Remote Sens. 103, 129–135.
Nepstad, D., McGrath, D., Stickler, C., Alencar, A., Azevedo, A., Swette, B., Bezerra, T., DiGiano, M., Shimada, J., da Motta, R.S., Armijo, E., Castello, L., Brando, P., Hansen, M.C., McGrath-Horn, M., Carvalho, O., Hess, L., 2014. Slowing Amazon deforestation through public policy and interventions in beef and soy supply chains. Science 344 (6188), 1118–1123.
Nobre, C.A., Obregón, G.O., Marengo, J.A., Fu, R., Poveda, G., 2009a. Characteristics of Amazonian climate: Main features. In Amazonia and Global Change, pp. 149–162, http://doi.org/10.1029/2008GM000720.
Nobre, C.A., Borma, L.D.S., 2009b. 'Tipping points' for the Amazon forest. Curr. Opin. Environ. Sustainab. 1 (1), 28–36.
Nobre, C.A., Sampaio, G., Borma, L.S., Castilla-Rubio, J.C., Silva, J.S., Cardoso, M., 2016. Land-use and climate change risks in the Amazon and the need of a novel sustainable development paradigm. PNAS 113 (39), 10759–10768. http://dx.doi.org/10.1073/pnas.1605516113.
Okin, G.S., Gu, J., 2015. The impact of atmospheric conditions and instrument noise on atmospheric correction and spectral mixture analysis of multispectral imagery. Remote Sens. Environ. 164, 130–141. http://dx.doi.org/10.1016/j.rse.2015.03.032.
Pacifico, F., Folberth, G.A., Sitch, S., Haywood, J.M., Rizzo, L.V., Malavelle, F.F., Artaxo, P., 2015. Biomass burning related ozone damage on vegetation over the Amazon forest: A model sensitivity study. Atmos. Chem. Phys. 15 (5), 2791–2804. http://dx.doi.org/10.5194/acp-15-2791-2015.
Park, E., Latrubesse, E.M., 2014. Modeling suspended sediment distribution patterns of the Amazon River using MODIS data. Remote Sens. Environ. 147, 232–242.
Phillips, O.L., Aragão, L.E., Lewis, S.L., Fisher, J.B., Lloyd, J., López-González, G., Van Der Heijden, G., 2009. Drought sensitivity of the Amazon rainforest. Science 323 (5919), 1344–1347.
Reddington, C.L., Butt, E.W., Ridley, D.A., Artaxo, P., Morgan, W.T., Coe, H., Spracklen, D.V., 2015. Air quality and human health improvements from reductions in deforestation-related fire in Brazil. Nat. Geosci. 8 (10), 768–771. http://dx.doi.org/10.1038/ngeo2535.
Royal Society, 2008. Ground-level ozone in the 21st century: future trends, impacts and policy implications. October. Retrieved from http://www.royalsociety.org/Ground-level-ozone-in-the-21st-century-future-trends-impacts-and-policy-implications-/.
Saleska, S.R., Didan, K., Huete, A.R., Da Rocha, H.R., 2007. Amazon forests green-up during 2005 drought. Science 318 (5850) 612 612.
Salomonson, V.V., Barnes, W.L., Maymon, P.W., Montgomery, H.E., Ostrow, H., 1989. MODIS: advanced facility instrument for studies of the earth as a system. IEEE Trans. Geosci. Remote Sens. 27 (2), 145–153. http://dx.doi.org/10.1109/36.20292.
Samanta, A., Ganguly, S., Hashimoto, H., Devadiga, S., Vermote, E., Knyazikhin, Y., Nemani, R.R., Myneni, R.B., 2010. Amazon forests did not green-up during the 2005 drought. Geophys. Res. Lett. 37 (5).
Samanta, A., Ganguly, S., Vermote, E., Nemani, R.R., Myneni, R.B., 2012. Why is remote sensing of amazon forest greenness so challenging? Earth Interact 16 (7), 1–14.
Sampaio, G., Nobre, C., Costa, M.H., Satyamurty, P., Soares-Filho, B.S., Cardoso, M., 2007. Regional climate change over eastern Amazonia caused by pasture and soybean cropland expansion. Geophys. Res. Lett. 34 (17), 1–7. http://dx.doi.org/10.1029/2007GL030612.

Sauvage, B., Martin, R.V., Van Donkelaar, A., Ziemke, J.R., 2007. Quantification of the factors controlling tropical tropospheric ozone and the South Atlantic maximum. J. Geophys. Res.: Atmospheres 112 (D11).

Schmid, B., Thorne, K.J., Demoulin, P., Peter, R., Mätzler, C., Sekler, J., 1996. Comparison of modeled and empirical approaches for retrieving columnar water vapor from solar transmittance measurements in the 0.94-μm region. J. Geophys. Res. : Atmospheres, 101(D5), 9345–9358. http://doi.org/10.1029/96JD00337.

Seemann, S.W., Li, J., Menzel, W.P., Gumley, L.E., 2003. Operational retrieval of atmospheric temperature, moisture, and ozone from MODIS infrared radiances. J. Appl. Meteorol. 42, 1072–1091. http://dx.doi.org/10.1175/1520-0450(2003)042<1072:OROATM>2.0.CO;2.

Sierra, J.P., Arias, P.A., Vieira, S.C., 2015. Precipitation over Northern South America and Its seasonal variability as simulated by the CMIP5 models. Adv. Meteorol. 2015, 1–22. http://dx.doi.org/10.1155/2015/634720.

Soares-Filho, B.S., Nepstad, D.C., Curran, L.M., Cerqueira, G.C., Garcia, R.A., Ramos, C.A., Schlesinger, P., 2006. Modelling conservation in the Amazon basin. Nature 440 (7083), 520.

Sobrino, J.A., Jiménez-Muñoz, J.C., Mattar, C., Sòria, G., 2015. Evaluation of Terra/MODIS atmospheric profiles product (MOD07) over the Iberian Peninsula: A comparison with radiosonde stations. Int. J. Digital Earth 8 (10), 771–783.

Smith, L.T., Aragao, L.E., Sabel, C.E., Nakaya, T., 2014. Drought impacts on children's respiratory health in the Brazilian Amazon. Sci. Rep., 4.

Spracklen, D.V., Arnold, S.R., Taylor, C.M., 2012. Observations of increased tropical rainfall preceded by air passage over forests. Nature 489 (7415), 282–285.

Tomasella, J., Borma, L.S., Marengo, J.A., Rodriguez, D.A., Cuartas, L.A., A Nobre, C., Prado, M.C., 2011. The droughts of 1996–1997 and 2004–2005 in Amazonia: hydrological response in the river main-stem. Hydrol. Process. 25 (8), 1228–1242.

Torres, O., Chen, Z., Jethva, H., Ahn, C., Freitas, S.R., Bhartia, P.K., 2010. OMI and MODIS observations of the anomalous 2008–2009 Southern Hemisphere biomass burning seasons. Atmos. Chem. Phys. 10 (8), 3505–3513.

Van Der Ent, R.J., Savenije, H.H.G., Schaefli, B., Steele-Dunne, S.C., 2010. Origin and fate of atmospheric moisture over continents. Water Resour. Res. 46 (9), 1–12. http://dx.doi.org/10.1029/2010WR009127.

Vera, C., Baez, J., Douglas, M., Emmanuel, C.B., Marengo, J., Meitin, J., Nicolini, J., Nogues-Paegle, J., Paegle, J., Penalba, O., Salio, P., Saulo, C., Silva Dias, M.A., Silva Dias, P., Zipser, E., 2006. The South American low-level jet experiment. Bull. Am. Meteorol. Soc. 87 (1), 63–77. http://dx.doi.org/10.1175/BAMS-87-1-63.

Vermote, E.F., Kotchenova, S., 2008. Atmospheric correction for the monitoring of land surfaces. J. Geophys. Res., 113(D23), D23S90. http://doi.org/10.1029/2007JD009662.

Vermote, E.F., Tanré, D., Deuzé, J.L., Herman, M., Morcrette, J.J., 1997. Second simulation of the satellite signal in the solar spectrum, 6s: an overview. IEEE Trans. Geosci. Remote Sens. 35 (3), 675–686. http://dx.doi.org/10.1109/36.581987.

Vuille, M., Burns, S.J., Taylor, B.L., Cruz, F.W., Bird, B.W., Abbott, M.B., Novello, V.F., 2012. A review of the South American monsoon history as recorded in stable isotopic proxies over the past two millennia. Clim. Past 8 (4), 1309–1321. http://dx.doi.org/10.5194/cp-8-1309-2012.

Wang, H., Fu, R., 2002. Cross-equatorial flow and seasonal cycle of precipitation over South America. J. Clim. 15 (13), 1591–1608.

Wiedinmyer, C., 2015. Atmospheric chemistry: Breathing easier in the Amazon. Nat. Geosci. 8 (10), 751–752. http://dx.doi.org/10.1038/ngeo2550.

Wilson, R.T., 2013. Py6S: A Python interface to the 6S radiative transfer model. Comput. Geosci. 51 (2), 166.

Wright, J.S., Fu, R., Worden, J.R., Chakraborty, S., Clinton, N.E., Risi, C., et al., 2017. Rainforest-initiated wet season onset over the southern Amazon. Proceedings of the National Academy of Sciences, 201621516.

Xu, L., Samanta, A., Costa, M.H., Ganguly, S., Nemani, R.R., Myneni, R.B., 2011. Widespread decline in greenness of Amazonian vegetation due to the 2010 drought. Geophys. Res. Lett. 38 (7).

Yang, J., Gong, P., Fu, R., Zhang, M., Chen, J., Liang, S., Dickinson, R., 2013. The role of satellite remote sensing in climate change studies. Nature Climate Change 3 (10), 875.

Yoon, Jin-Ho, Zeng, Ning, 2010. An Atlantic influence on Amazon rainfall. Clim. Dyn. 34 (2–3), 249–264.

Zelazowski, P., Sayer, A., Thomas, G.E., Grainger, R.G., 2011. Reconciling satellite-derived atmospheric properties with fine-resolution land imagery: Insights for atmospheric correction. J. Retrieved from http://onlinelibrary.wiley.com/doi/10.1029/2010JD015488/full.

Ziemke, J.R., Chandra, S., Duncan, B.N., Schoeberl, M.R., Torres, O., Damon, M.R., Bhartia, P.K., 2009. Recent biomass burning in the tropics and related changes in tropospheric ozone. Geophys. Res. Lett. 36 (15), 1–5. http://dx.doi.org/10.1029/2009GL039303.

Ziemke, J.R., Chandra, S., Labow, G.J., Bhartia, P.K., Froidevaux, L., Witte, J.C., 2011. A global climatology of tropospheric and stratospheric ozone derived from Aura OMI and MLS measurements. Atmos. Chem. Phys. 11 (17), 9237–9251.

Zhu, Z., 2017. Change detection using landsat time series: A review of frequencies, preprocessing, algorithms, and applications. ISPRS J. Photogramm. Remote Sens. 130, 370–384.